

## Article

# Assessment of Meteorological and Agricultural Drought Indices under Climate Change Scenarios in the South Saskatchewan River Basin, Canada

Mohammad Zare <sup>1</sup>, Shahid Azam <sup>2,\*</sup> , David Sauchyn <sup>1</sup>  and Soumik Basu <sup>1,3</sup> <sup>1</sup> Prairie Adaptations Research Collaborative, University of Regina, Regina, SK S4S 0A2, Canada<sup>2</sup> Environmental Systems Engineering, University of Regina, Regina, SK S4S 0A2, Canada<sup>3</sup> International Arctic Research Center, University of Alaska Fairbanks, Fairbanks, AK 99775, USA

\* Correspondence: shahid.azam@uregina.ca

**Abstract:** Climate change has amplified the severity of droughts with potentially adverse impacts on agriculture in western Canada. This study assessed meteorological and agricultural drought in the Southern Saskatchewan River Basin (SSRB) using an array of drought indices, including the Standardized Precipitation Index (SPI), the Standardized Precipitation-Evapotranspiration Index (SPEI), the Self-Calibrated Palmer Drought Severity Index (scPDSI), the Soil Moisture Deficit Index (SMDI), and the Evapotranspiration Deficit Index (ETDI). These indices were evaluated using multiple regional climate model (RCM) projections assuming 1.5, 2.0, and 3.0 °C thresholds of global warming. A modified Soil and Water Assessment Tool (SWAT-M) was used to simulate the soil water content (SWC), actual evapotranspiration (AET), and potential evapotranspiration. The results of a sensitivity analysis using the SUFI-2 method in SWAT-CUP showed that the model performed well with BIAS lower than 10% and NSE and R higher than 0.7, and the range of SWC output closely matched the observed SWC. According to the RCM projections, the annual precipitation increases for all three global temperature thresholds while the annual mean temperature increases at a greater rate than the rise in global mean temperature. The projected PDSI and the SPEI suggest that drought duration and severity will exceed historical values while SPI will remain largely unchanged. Furthermore, severe drought conditions (SMDI < 2.0) are more frequent under the 3.0 °C global temperature scenario. The mean ETDI was historically 0.58 while the projected value is 0.2, 0.1, and −0.2 for the first to third scenarios, respectively. Simulated values, spatial maps, and heat maps of SMDI and ETDI illustrated that Canesm2.CRCM5 projects the driest conditions among all the RCMs. Agricultural drought indices, which incorporate SWC data, show more significant effects than meteorological drought indices. The increasing dryness will potentially impact agricultural crop production, particularly under the third scenario (3 °C) in the SSRB.

**Keywords:** drought indices; climate change; SWC; SWAT-M; Southern Saskatchewan River Basin

check for updates

**Citation:** Zare, M.; Azam, S.; Sauchyn, D.; Basu, S. Assessment of Meteorological and Agricultural Drought Indices under Climate Change Scenarios in the South Saskatchewan River Basin, Canada. *Sustainability* **2023**, *15*, 5907. <https://doi.org/10.3390/su15075907>

Academic Editor: Teodor Rusu

Received: 14 January 2023

Revised: 9 March 2023

Accepted: 27 March 2023

Published: 29 March 2023



**Copyright:** © 2023 by the authors. Licensee MDPI, Basel, Switzerland. This article is an open access article distributed under the terms and conditions of the Creative Commons Attribution (CC BY) license (<https://creativecommons.org/licenses/by/4.0/>).

## 1. Introduction

Drought is a slowly developing natural disaster related to regional climatic variability and it is unlike aridity, which is a permanent climate phenomenon of low precipitation [1]. Drought is commonly categorized as meteorological, agricultural, hydrological, and socio-economic [2]. This classification is based on the number of days below a particular rainfall threshold for meteorological drought, soil moisture deficits, and evaporation stress for agricultural drought, or on the levels of surface and groundwater supplies for hydrological drought indices [3,4]. Therefore, hydro-meteorological variables, including streamflow and soil moisture, are used to detect and monitor drier than normal conditions [5]. Drought ultimately has socioeconomic consequences [6–8]. The severity and frequency of drought are expected to increase with global climate change. The annual average temperature of Canada has increased by about 1.7 °C relative to 1984–2016 (approximately double the

global mean increase) and 1.9 °C across the Prairies, where the Southern Saskatchewan River Basin (SSRB) is located [9]. According to the high emission representative concentration pathway (RCP) 8.5, the annual mean temperature in the Canadian Prairies could rise up to 2.3 and 6.5 °C by 2031 to 2050 and 2081 to 2100, respectively, compared with 1986–2005 [10]. The SSRB is characterized by relatively low precipitation due to the atmospheric flow barrier imposed by the Rocky Mountains [11]. This region is prone to frequent and severe droughts [12]. Since drought is predominantly controlled by air temperature and precipitation [13], climate changes could lead to serious risks for this region. The Prairies cover about 80% of Canada's agricultural lands [14] and largely account for Canada's status as the world's fifth-largest exporter of agricultural products and the world's largest exporter of canola for human consumption [15]. Fluctuations in precipitation, temperature, and consequently, soil moisture, play a major role in the annual dryland crop production.

Multi-year droughts occurred periodically in the historical record [16,17] and, in particular, prior to the instrumented period [18]. Several studies have examined meteorological, agricultural, and hydrological droughts in the region [19–23], mostly using drought indices, such as the Standardized Precipitation Index (SPI) and the Standardized Precipitation Evapotranspiration Index (SPEI). Although climate change plays a vital role in the probability and severity of drought, few studies have applied drought indicators to the problem of climate change in this area. Masud et al. [24] used a NARCCAP multi-RCM ensemble to examine drought characteristics over the Canadian Prairies via SPI and SPEI. Their findings confirm high drought vulnerability over the southern and southwestern parts of Prairies. Bonsal et al. [25] extracted SPEI data from 29 global climate models (GCMs) and three representative concentration pathways (RCPs) and concluded that the duration and intensity of future severe droughts would increase due to longer persistence stages, whereas growth and retreat stages are largely shorter. The main limitation of these approaches is the treatment of droughts on fixed scales with little attention to temporal and spatial evolution that use only one or two agricultural indices [26].

Climate model projections for this region consistently include decreased summer precipitation and a longer annual period of net positive evapotranspiration [9,27]. Therefore, we undertook research using data from regional climate models to evaluate changes in indices of meteorological and agricultural drought. The novelty of this study is our approach for the assessment of drought indices based on global warming scenarios (1.5, 2, and 3 °C relative to the historical period (1975–2004)) for individual RCMs. Furthermore, we focused on drought indices based on the output from a hydrological model: the SWAT-modified (SWAT-M) model output (SWC and AET) [28]. The objectives of this study include the following: (i) to verify the SWAT-M model outputs for hydrological variables against observational data; (ii) to compare several drought indices according to timelines of mean global temperature increases of 1.5 °C, 2.0 °C, and 3.0 °C, with respect to historical condition among different NA-CORDEX RCM models; and (iii) to investigate spatiotemporal linkages between drought and climate change.

## 2. Research Methodology

### 2.1. Study Area

The study area is the South Saskatchewan River Basin, which spans two provinces, Alberta and Saskatchewan, with a total drainage area of 168,000 km<sup>2</sup> that includes 4 sub-basins: Red Deer River (RDR), Bow River (BR), Oldman River (OR), and Lower SSR (LSSR) (Figure 1). This region encompasses diversified landscapes varying from the front range of the Rocky Mountains to relatively low-relief topography in the eastern part, with elevations from about 3485 m above sea level in the west to 376 m in the east. The SSRB is characterized by a semi-arid continental climate with cold, dry winters and hot, humid summers, with snowmelt runoff occurring in spring [26]. Precipitation is low because the SSRB is located on the leeward side of the Rocky Mountains [29] such that annual precipitation in the southern areas of Saskatchewan and Alberta is about 300 to 400 mm. This region has strong seasonality with annual mean temperature ranging from 14 °C to 16 °C in summer and

−2.5 °C to −8 °C in winter [30]. Agriculture is the main land use; 58% of the SSRB is cropland, accounting for around 80% of Canadian agricultural production [14]. Drought from many single to multi years, particularly during 1999–2005 [31], has periodically affected crop yield in the region.

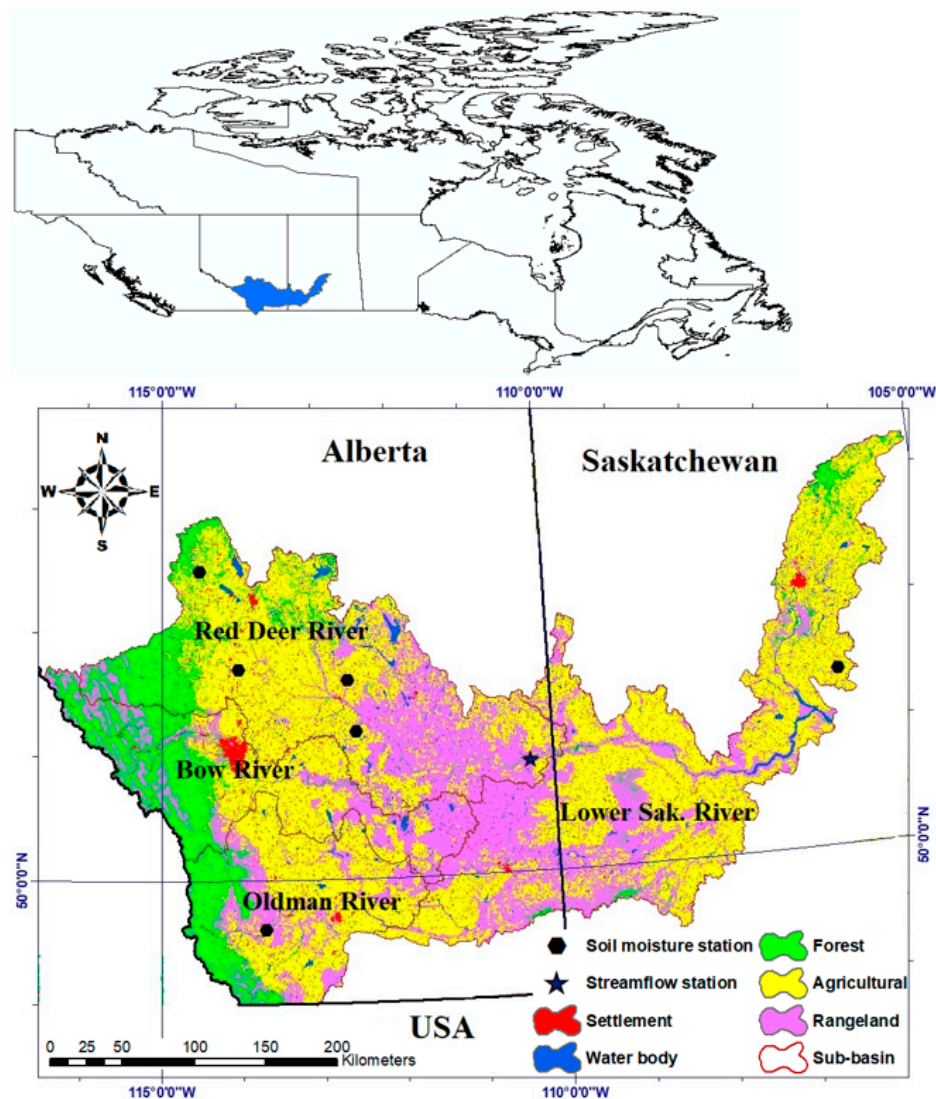


**Figure 1.** Locations soil moisture and streamflow stations in SSRB (after Zare et al. [28]).

## 2.2. Datasets

Daily precipitation, minimum and maximum temperature, solar radiation, wind speed, and relative humidity from 1991 to 2020 at 17 meteorological stations were retrieved from Environment and Climate Change Canada (ECCC). Likewise, daily stream discharge data of the SWAT model were used for calibration (1993–2005) and validation (2006–2013) and daily measured soil moisture was used for calibrating SWC in the SWAT model from April 2015 to September 2020 (warm season). Land-use data for 2015 were retrieved from the Soil Landscapes of Canada (SLC ver. 3.2), whereas topographic data were derived from a 20 m resolution Digital Elevation Model (Canadian GeoGratis) for watershed delineation. Table 1 summarizes the input data used for hydrological modeling in the Arc SWAT interface.

**Table 1.** Input data used in SWAT model (after Zare et al. [28]).

Data Type	Description	Information	Source
Digital Elevation Model	Watershed delineation	Raster, 30 m resolution	<a href="http://geogratis.gc.ca">http://geogratis.gc.ca</a> accessed 8 September 2022
Land use	Land-use classification	Raster, 30 m resolution	<a href="http://geogratis.gc.ca">http://geogratis.gc.ca</a> accessed 14 September 2022
Soil type	Soil properties	Vector	<a href="http://www.agr.gc.ca">http://www.agr.gc.ca</a> accessed 27 September 2022
Weather	Precipitation and temperature	Daily	<a href="https://weather.gc.ca">https://weather.gc.ca</a> accessed 15 August 2022
Streamflow measured	Calibration and validation	Daily	<a href="https://wateroffice.ec.gc.ca">https://wateroffice.ec.gc.ca</a> accessed 29 August 2022
Soil moisture measured	Calibration model	Daily	<a href="https://acis.alberta.ca">https://acis.alberta.ca</a> accessed 3 September 2022

The North American-Coordinated Regional Climate Downscaling Experiment (NA-CORDEX) was the source of climate model data. The NA-CORDEX project uses output from experiments that paired global climate models (GCM) from the Coupled Model Inter-comparison Project Phase 5 (CMIP5) with a set of regional climate models (RCM) over the North American domain [32]. Thus, NA-CORDEX is based on the use of various RCMs to dynamically downscale state-of-the-art GCMs from the CMIP5 (Table 2).

**Table 2.** Summary of NA-CORDEX simulations.

Simulation Name	GCM Derived	RCM Model Name	Institute
CanESM2.CanRCM4	CanESM2	Canadian Regional Climate Model version 4	Canadian Centre for Climate Modelling and Analysis (CCCma)
CanESM2.CRCM5	CanESM2	Canadian Regional Climate Model (CRCM) version 5	Université du Québec à Montréal (UQAM)
GEMatm-Can.CRCM5	GEMatm	Canadian Regional Climate Model (CRCM) version 5	Université du Québec à Montréal (UQAM)
GEMatm-MPI.CRCM5	GEMatm	Canadian Regional Climate Model (CRCM) version 5	Université du Québec à Montréal (UQAM)
GFDL-ESM2M.RegCM4	GFDL-ESM2	Regional Climate Model version 4	Iowa State University and National Center for Atmospheric Research (NCAR)
GFDL-ESM2M.WRF	GFDL-ESM2	Weather Research and Forecast model	University of Arizona and NCAR
HadGEM2-ES.WRF	HadGEM2-ES	Weather Research and Forecast model	University of Arizona and NCAR
MPI-ESM-LR.CRCM5	MPI-ESM-LR	Canadian Regional Climate Model (CRCM) version 5	Université du Québec à Montréal (UQAM)
MPI-ESM-LR.RegCM4	MPI-ESM-LR	Regional Climate Model version 4	Iowa State University and National Center for Atmospheric Research (NCAR)
MPI-ESM-LR.WRF	MPI-ESM-LR	Weather Research and Forecast model	University of Arizona and NCAR
MPI-ESM-MR.CRCM5	MPI-ESM-MR	Canadian Regional Climate Model (CRCM) version 5	Université du Québec à Montréal (UQAM)

Our analysis of drought indices is based on 10 simulations from the CORDEX ensemble at 0.22°, which is ~25 km spatial resolution and using the RCP8.5 emission scenario to define 30-year periods centered on the global warming levels of 1.5, 2, and 3 °C, as shown in

Table 3. The dynamically downscaled model outputs for North America is not yet available for SSP scenarios. Furthermore, the years of global warming levels are based on the 11-year running average of the global mean surface air temperature changes in the future. The periods were calculated from the global mean surface air temperature increase in RCP 8.5. For this purpose, the 11-year running average of global mean surface air temperature was calculated and then anomalies from historical period were calculated. The temperature increases due to global warming were not linear, so the 11-year running mean was used. For example, if in 2060 the temperature increase crosses 2 °C threshold, the period would be 2060 ± 15 years, hence 2045–2075. The periods were calculated for each of the GCMs involved. The effect of various warming levels on regional drought scenarios was expressed as the shifts in drought indices between the future 30-year periods and a historical baseline period (1975–2004). The model output, ‘mbcn-Daymet’ was bias-corrected using the MBCn algorithm against Daymet gridded observational datasets [33].

**Table 3.** Time for GCM models to reach various levels of thresholds of temperature relative to historical period under RCP8.5.

GCMs Model	1.5 °C	2.0 °C	3.0 °C
CanESM2	2016–2045	2028–2057	2047–2076
MPI-ESM-LR	2029–2058	2041–2070	2063–2092
MPI-ESM-MR	2030–2059	2040–2069	2061–2090
GFDL-ESM2	2023–2052	2038–2067	2068–2097
HadGEM2-ES	2003–2032	2016–2045	2037–2066
GEM.Can	2016–2045	2028–2057	2047–2076
GEM.MPI	2029–2058	2041–2070	2063–2092

### 2.3. Drought Indices

We considered five drought indices based on two categories of meteorological (SPI, SPEI, and PDSI) and agricultural drought (SMDI and ETDI) in order to comprehensively assess future changes in long-term drought under different degrees of global warming. Figure 2 provides the flow chart of the modeling process.

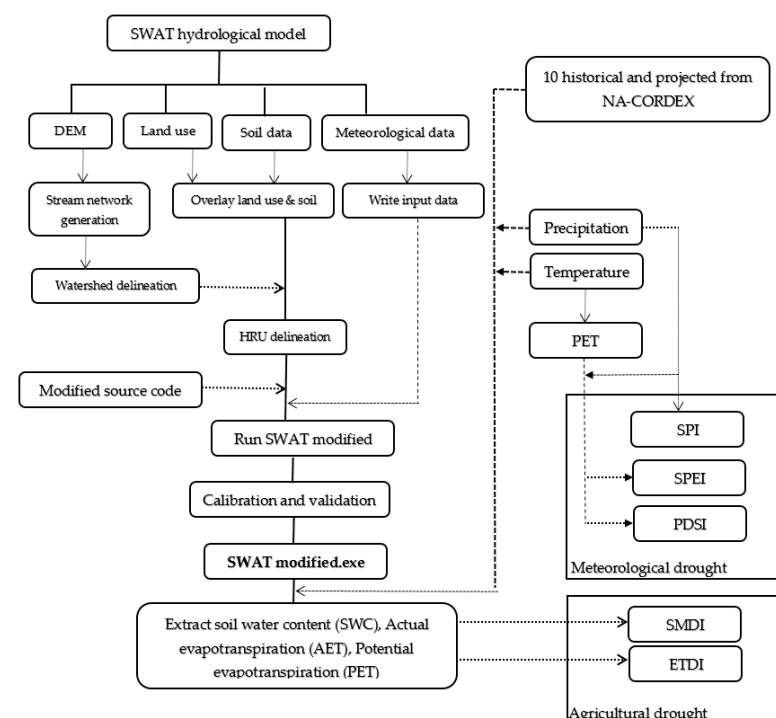


**Figure 2.** Modeling framework designed in this study.

a. Standardized Precipitation Index (SPI)

The SPI allows monitoring and analysis of meteorological drought through the transformation of aggregated rainfall data at different time scales [34]. SPI is a statistical monthly indicator (e.g., 3, 6, 12, and 24 months) that is fitted to a long-term precipitation time series using a gamma distribution function, as given by the following equation [35,36]:

$$f(x; \alpha, \beta) = \frac{1}{\beta^\alpha \int_0^\infty x^{\alpha-1} e^{-x/\beta} dx} x^{\alpha-1} e^{-x/\beta}, \quad \text{for } x > 0 \quad (1)$$

where,  $x$  is monthly precipitation,  $\alpha$  and  $\beta$  are shape and scale parameters of the probability distribution, respectively. The SPI time series gives positive or negative precipitation anomalies as the basis for defining drought events [34] (Table 4).

**Table 4.** Thresholds of SPI, SPEI, and PDSI for wet and dry periods.

SPI and SPEI Value	PDSI Value	Class
Greater than 2.00	Greater than 4.00	Extremely wet
1.50 to 1.99	3.00 to 3.99	Severely wet
1.00 to 1.49	2.00 to 2.99	Moderately wet
0.50 to 0.99	1.00 to 1.99	Slightly wet
−0.49 to 0.49	−0.99 to 0.99	Near normal
−0.99 to −0.50	−1.99 to −1.00	Mild dry
−1.49 to −1.00	−2.99 to −2.00	Moderately dry
−1.99 to −1.5	−3.99 to −3.00	Severely dry
Less than −2.00	Less than −4.00	Extremely dry

b. Standardized precipitation evaporation index (SPEI)

SPEI is a meteorological drought index, which takes into account the difference between monthly precipitation and reference evapotranspiration demand of the atmosphere [37]. Several studies confirm that this index is suitable for drought assessment under the effect of climate change as it captures the influence of potential evapotranspiration (PET) on drought severity [28,38–41]. SPEI is computed by simple subtraction as given in following equation:

$$D_i = P_i - PET_i \quad (2)$$

where,  $P$  is the monthly precipitation (mm) and PET is the potential evapotranspiration (mm) for  $i$  months. Vicente-Serrano et al. [37], proposed a method to estimate  $D_i$  values using the default three-parameter log-logistic distribution function instead of a two-parameter gamma distribution function needed for SPI [42]. The probability density function (pdf) ( $f(x)$ ) of the three-parameter log-log distribution variable is defined by Equation (3):

$$f(x) = \frac{\beta}{\alpha} \left( \frac{x-y}{\alpha} \right) \left[ 1 + \frac{x-y}{\alpha} \right]^{-2} \quad (3)$$

where,  $\alpha$ ,  $\beta$ , and  $y$  are the scale, shape, and origin parameters, respectively, which are obtained using the L-moment procedure for  $D$  values in the range ( $y > D > \infty$ ). Therefore, the PDF of the  $D$  series is given by the following equation:

$$F(x) = \left[ 1 + \left( \frac{\alpha}{x-y} \right)^\beta \right]^{-1} \quad (4)$$

SPEI values were calculated as the standardized values of  $F(x)$  following Abramowitz and Stegun. [43] and details by Vicente-Serrano et al. [37] using the following equation:

$$SPEI = W - \frac{C_0 + C_1 W + C_2 W^2}{1 + d_1 W + d_2 W^2 + d_3 W^3} \quad (5)$$

where,  $W = \sqrt{-2\ln(p)}$  for  $P \leq 0.5$  and  $P$  is the exceeding probability determined by the  $D$  value,  $P = 1 - F(x)$ . If  $P > 0.5$ , then  $P$  is used to replace by  $1 - P$  and the sign of the resultant SPEI is reversed. The constants are  $C_0 = 2.515517$ ,  $C_1 = 0.802853$ ,  $C_2 = 0.010328$ ,  $d_1 = 1.432788$ ,  $d_2 = 0.189269$ , and  $d_3 = 0.001308$ . The definition of a drought event using the SPEI is similar to SPI (Table 4).

c. Self-Calibrated Palmer Drought Severity Index (scPDSI)

The Self-Calibrated Palmer Drought Severity Index (scPDSI) calibrates the PDSI for the location of interest based on water demand and supply instead of simply variation in rainfall (Wells et al., 2004 [44]). This index employs three factors: rainfall, temperature, and locally available soil water capacity (SWC). The variables of evapotranspiration (ET), recharge (R), runoff (RO), potential recharge (PR), potential evapotranspiration (PET), loss (L), potential runoff (PR), and potential loss (PL) are estimated for AWC. These four variables are weighted according to the regional climate. The weighting factors,  $\alpha$ ,  $\beta$ ,  $\gamma$ , and  $\delta$ , are water-balanced coefficients calculated using the following equations:

$$\alpha = \frac{ET}{PET} \quad \beta = \frac{R}{PR} \quad \gamma = \frac{RO}{PR} \quad \delta = \frac{L}{PL} \quad (6)$$

where,  $E$ ,  $R$ ,  $RO$ , and  $L$  represent evaporation, soils recharge, runoff, and water loss of the soil layer, and their potential values are  $PE$ ,  $PR$ ,  $PRO$ ,  $PL$ , respectively, so that the variables rely on the soil AWC.

$$p = \alpha PET + \beta PR + \gamma PRO - \delta PL \quad (7)$$

where,  $p$  is the amount of precipitation required to maintain a normal soil moisture level for a particular month under consideration.

Following Palmer's algorithm [8,44,45], the moisture departure ( $d$ ) was derived from the difference between one month of rainfall ( $p$ ) under normal conditions and evapotranspiration estimation ( $ET$ ). The monthly moisture anomaly index ( $Z$  index) for a given location and time period indicates the degree of dryness or wetness without considering recent rainfall trends:

$$Z = dK \quad (8)$$

where,  $K$  is the climate coefficient characteristic of the location:

$$K = \frac{17.67}{\sum_{j=1}^{12} d_j K_j} K_j \quad (9)$$

The only difference between the PDSI and scPDSI is the replacement of the empirically derived climatic characteristic ( $K$ ) and duration factors (0.897 and 1/3), with values calculated automatically using historical climatic data for the study area. Monthly scPDSI values were estimated for all of the meteorological stations in the SSRB using the homogenized monthly precipitation and PET (Penman method) for the historical and projected periods. This drought index classification, ranging from negative to positive values, is shown in Table 4.

d. Soil Moisture Deficit Index (SMDI).

The SMDI is based on the soil water content (SWC) anomaly during a given time step (i.e., week, month). The long-term SWC for each month was obtained by taking the median, maximum, and minimum values from 10 RCMs during the historical and projection periods. Following Narasimhan and Srinivasan [46], the median was chosen over the mean as a measure of "normal" SWC because the median is more stable and is not influenced by outliers. SMDI values for 30-year historical and future periods were obtained by the following set of equations:

$$SD_{i,j} = \frac{SW_{i,j} - MSW_j}{MSW_j - \min SW_j} \times 100, \quad \text{if } SW_{i,j} \leq MSW_j,$$

$$SD_{i,j} = \frac{SW_{i,j} - MSW_j}{maxSW_j - MSW_j} \times 100, \text{ if } SW_{i,j} > MSW_j, \quad (10)$$

$$SMDI_j = 0.5SMDI_{j-1} + \frac{SD_j}{50} \quad (11)$$

where,  $SD_{i,j}$  is soil water deficit (%),  $SW_{i,j}$  is the mean monthly SWC in the soil profile (mm),  $MSW_j$  is the long-term median SWC (mm),  $minSW_j$  and  $maxSW_j$  are the long-term minimum and maximum SWC (mm),  $i$  is the year, and  $j$  is the month. SMDI ranges from  $-2$  to  $+2$ , with negative values referring to drought. In the current study, the Soil and Water Assessment Tool (SWAT) was used as a hydrologic model to simulate SWC [28].

#### e. Evapotranspiration Deficit Index (ETDI)

The ETDI was calculated using a procedure similar to the one explained above for SMDI; however, it is based on the water stress anomaly relative to its long-term average. In this study, the monthly SWAT model's output of actual evapotranspiration (AET) and potential evapotranspiration (PET) was achieved using the median, maximum, and minimum values from the historical and projected 10 RCM simulations. The monthly water stress ratio is calculated using Equation (12):

$$WS = \frac{PET - AET}{PET} \quad (12)$$

where  $WS$  is the monthly water stress ratio,  $PET$  is the monthly potential evapotranspiration, and  $AET$  is the monthly actual evapotranspiration. Next, monthly long-term ETDI is calculated using the following equations:

$$WSA_{i,j} = \frac{MWS_{i,j} - WS_j}{MWS_j - minWS_j} \times 100, \text{ if } WS_{i,j} \leq MWS_j,$$

$$WSA_{i,j} = \frac{MWS_{i,j} - WS_j}{maxWS_j - MWS_j} \times 100, \text{ if } WS_{i,j} > MWS_j, \quad (13)$$

$$ETDI_j = 0.5ETDI_{j-1} + \frac{WSA_j}{50} \quad (14)$$

where,  $WSA_{i,j}$  is monthly water stress anomaly,  $MWS_{i,j}$ ,  $minWS_j$ , and  $maxWS_j$  are median, minimum, and maximum water stress (mm), respectively. The thresholds of agriculture drought resulting from SMDI and ETDI are shown in Table 5.

**Table 5.** Thresholds of SMDI and ETDI for wet and dry periods.

SMDI and ETDI	Class
Greater than 2.00	Extremely wet
1.50 to 1.99	Severely wet
1.00 to 1.49	Moderately wet
$-0.99$ to $0.99$	Near normal
$-1.49$ to $-1.00$	Moderately dry
$-1.99$ to $-1.5$	Severely dry
Less than $-2.00$	Extremely dry

The indices described above enable the assessment of drought duration, severity, and intensity [47]. Drought duration (m) refers to the number of months between the starting (included) and ending (not included) months. Drought severity ( $S_e$ ) is the absolute value of the sum of index values during a drought event [48,49]. We used the three indices SPI, SPEI, and scPDSI and the corresponding drought thresholds to determine duration and severity. Drought duration is the period during which the SPI, SPEI, and scPDSI are

continuously negative, starting from the threshold values of  $-1$  and ending with positive values. Drought severity is the cumulative SPI, SPEI, and scPDSI values over the drought duration, while intensity is the ratio of drought severity to duration as given below.

$$S_e = \left| \sum_{j=1}^m Index_j \right|_e \quad (15)$$

where  $e$  is a drought event;  $j$  is a month;  $Index_j$  is the SPI, SPEI, and scPDSI values in month  $j$ ; and  $m$  and  $S_e$  are the duration and severity of a drought even, respectively.

#### 2.4. Hydrologic Modeling

A novel aspect of this study was the use of the spatially distributed Soil and Water Assessment Tool (SWAT) model for developing the agricultural drought index data. SWAT is a model of catchment hydrology. Sub-basins are delineated based on land use as well as soil type and slope, all of which are discretized into hydrologic response units (HRUs). SWAT is a temporally continuous, semi-distributed, and physically based model that uses daily, monthly, and yearly time steps to simulate physical processes of climate, soil moisture, plant growth, nutrients, pesticides, bacteria and pathogens, and soil management [50]. Hydrologic cycle in SWAT was based on the following form of the water balance equation:

$$SW_t = SW_o + \sum_{i=1}^t (R_{day} - Q_{surf} - E_a - W_{seep} - Q_{gw})_i \quad (16)$$

where  $SW_t$  is the final soil water content (mm),  $SW_o$  is the initial soil water content on day  $i$  (mm),  $t$  is the time (days),  $R_{day}$  is the daily precipitation  $i$  (mm),  $Q_{surf}$  is the daily surface runoff (mm),  $E_a$  is the daily evapotranspiration  $i$  (mm water),  $W_{seep}$  is the amount of water entering the vadose zone from the soil profile bottom layer on day  $i$  (mm), and  $Q_{gw}$  is the amount of return flow on day  $i$  (mm). A total of 4873 HRUs were delineated by defining thresholds of 2% for land use and 5% for soil type. Moreover, Penman–Monteith method was used to estimate the potential evaporation. In this study, we applied multi-step calibration that included streamflow [50] and soil moisture by measuring data for each variable [51,52]. The SWAT-CUP and the Sequential Uncertainty Fitting (SUFI-2) program [53] were used to conduct sensitivity, calibration, and uncertainty analyses of the model. Monthly simulated and observed flows during the calibration period (1993–2005) and validation period (2006–2013) were used by three statistics to evaluate the model performance: the Nash–Sutcliffe efficiency (NSE) [54], the percent bias (PBIAS) [55], and the coefficient of correlation ( $r$ ) [56] according to the following set of equations:

$$NSE = \left[ 1 - \frac{\sum_{i=1}^n (Q_i^{obs} - \bar{Q}_i^{sim})^2}{\sum_{i=1}^n (Q_i^{obs} - Q_{mean}^{obs})^2} \right] \quad (17)$$

$$PBIAS = \frac{\sum_{i=1}^n (Q_i^{obs} - Q_i^{sim})}{\sum_{i=1}^n Q_i^{obs}} \times 100 \quad (18)$$

$$r = \frac{\sum_{i=1}^n (Q_i^{obs} - \bar{Q}_i^{obs}) \cdot (Q_i^{sim} - \bar{Q}_i^{sim})}{\sqrt{\sum_{i=1}^n (Q_i^{obs} - \bar{Q}_i^{obs})^2} \cdot \sqrt{\sum_{i=1}^n (Q_i^{sim} - \bar{Q}_i^{sim})^2}} \quad (19)$$

where,  $\bar{Q}_i^{sim}$  and  $\bar{Q}_i^{obs}$  are the mean monthly simulated and observed discharge,  $Q_i^{obs}$  is observed discharge on the  $i$ th day,  $Q_i^{sim}$  is the simulated monthly discharge,  $n$  is the total number of months, and  $Q_{mean}^{obs}$  is the average observed monthly streamflow. According to Zare et al. [26], SWAT modeling has limitations when applied to cold regions, where

streamflow is predominantly generated by melting snow during spring. Streamflow is underestimated due to an abrupt increase during the thawing time. Likewise, rain-on-snow (ROS) events occasionally occur in the SSRB during winter and are frequently observed in spring. These events create uncertainty for model performances in regional watersheds because runoff from snowmelt is not homogeneous at the watershed scale [57]. Therefore, SWAT source code needs to be modified for cold regions. We used a combination of the physically based soil temperature module (not empirical) along with an energy budget equation for snowmelt for ROS events. In essence, the modified version of SWAT is capable to simulate freeze–thaw cycles and variation of frozen water content in soils. As such, this module closely simulates streamflow and soil temperature in cold weather. Detailed information regarding SWAT modification, including functions and variables, was given in Zare et al. [28].

### 3. Results

#### 3.1. Uncertainty, Sensitivity, and Calibration

The results of the SUFI-2 method's sensitivity analysis and calibration of the SWAT simulation of streamflow, SWC, and snowmelt for a period of 19 years is shown in Figure 3. The 18 most sensitive among the 30 input parameters have the highest t-values and the most significance ( $p$ -values approaching zero). The data indicate that the curve number at the moisture condition (CN2) was the most sensitive (high t-values); the most significant ( $p$ -values approaching zero) were followed by soil water content (SOL\_AWC), land use and soil's permeability [58–61]. The most sensitive and significant values of CN2 show that there is high runoff potential in the SSRB. The eight parameters with  $p < 0.5$  played an important role in the SWAT simulation on streamflow, soil moisture and snowmelt.

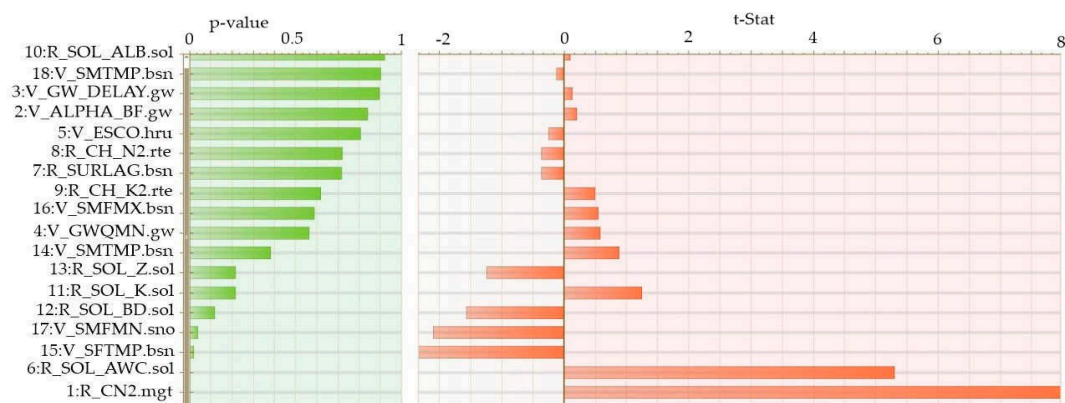


**Figure 3.** Performance indices of SWAT-M model parameters in the SSRB.

Calibration and validation results from SUFI-2 comparing observed and simulated streamflow from 1993 to 2005 and 2006 to 2013 are given in Figure 4. The NSE values are 0.71 and 0.76 for the calibration and validation periods. Values of NSE greater than 0.5 indicate that the SWAT model's performance is adequate for the monthly time step [62]. Similarly, relatively high values of  $r$  (0.83 and 0.88 for calibration and validation, respectively) confirm a good correlation between the observed and simulated streamflow. PBIAS values ranged from  $-9.3\%$  to  $-8.4\%$  for the two periods, suggesting a very good performance ( $(\text{PBIAS} < \pm 10\%)$ ) [53,63,64]. These results confirm that the SWAT model is able to simulate streamflow relative to measured values.

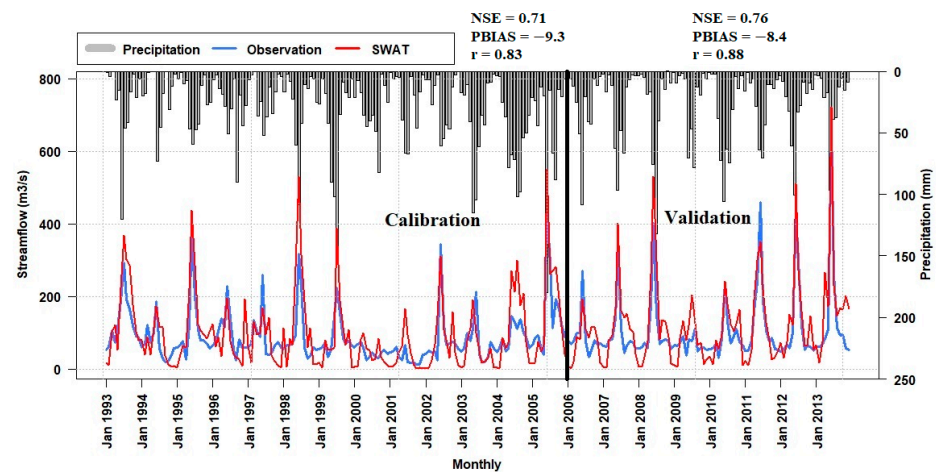


**Figure 4.** Monthly simulated and observed flows during the calibration period (1993–2005) and validation period (2006–2013) for SWAT-M (after Zare et al. [28]).

Table 6 summarizes the statistical performance of the SWAT model for the warm season based on daily measurement data from six stations and three error metrics (i.e., NSE, PBIAS, and *r*). The average correlation coefficient between field measurement and SWAT products was 0.51. Moreover, the average of PBIAS indices for all stations revealed that the SWAT model simulation was a good fit ( $\pm 10\% \leq \text{PBIAS} \leq \pm 15\%$ ) to measured SWC. Moreover, a daily time series (warm season) of simulated SWC and observations during the calibration period show that an agreement validates the ability of the SWAT to model SWC (Figure 5).

**Table 6.** Daily statistical analysis between SWAT-M with measurement data for SWAT.

Statistical Indices	<i>r</i>	PBIAS	NSE
Hussar	0.55	9.5	0.72
Morrin	0.53	−10.2	0.79
Old college	0.45	−9.1	0.61
Leedale	0.33	15.7	0.57
Brocket	0.57	−8.2	0.86
Kenaston	0.65	7.1	0.78
Mean	0.51	10	0.72

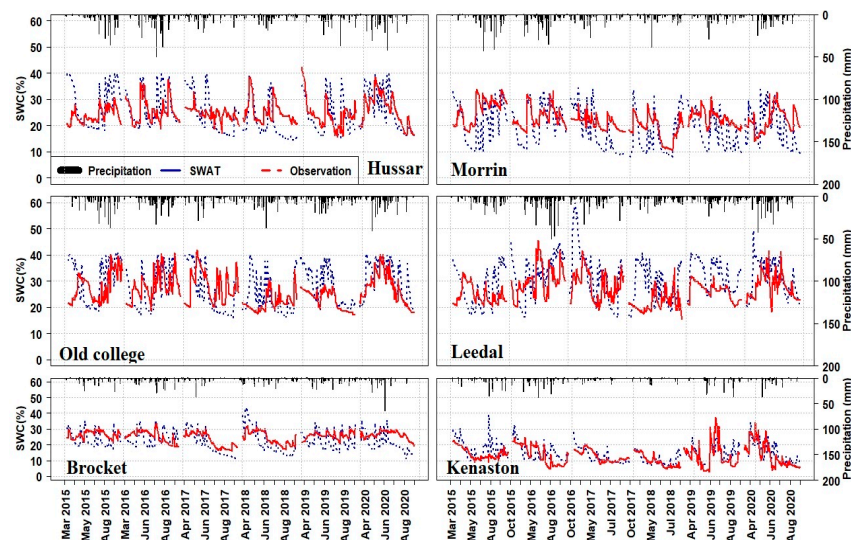


**Figure 5.** Temporal comparison of soil water content for SWAT m in a different station (after Zare et al. [28]).

### 3.2. Impact of Climate Change on Weather Parameters

The scatter plots of projected changes in the mean temperature and total precipitation between future and historical periods under three different global temperature thresholds show that the multi-RCM mean precipitation increased by 8%, 7%, and 9% for the 1.5 °C, 2 °C, and 3 °C scenarios, respectively, when compared with the historical period (Figure 6). The annual changes in precipitation are positive for all three global temperature thresholds except for CanESM2.CRCM5 in the first and third scenarios along with MPI-ESM-LR.CRCM5 for the second scenario. The largest increases in precipitation are under 3 °C, ranging between −1.88 and 23% among the different RCMs. The precipitation increases are approximately similar for 1.5 °C and 2 °C. The annual mean temperature increases from 1.5 to 3.1 degrees under 1.5 °C, 1.9, to 3.5 degrees at 2 °C and 3 to 4.5 degrees with 3 °C of global warming.

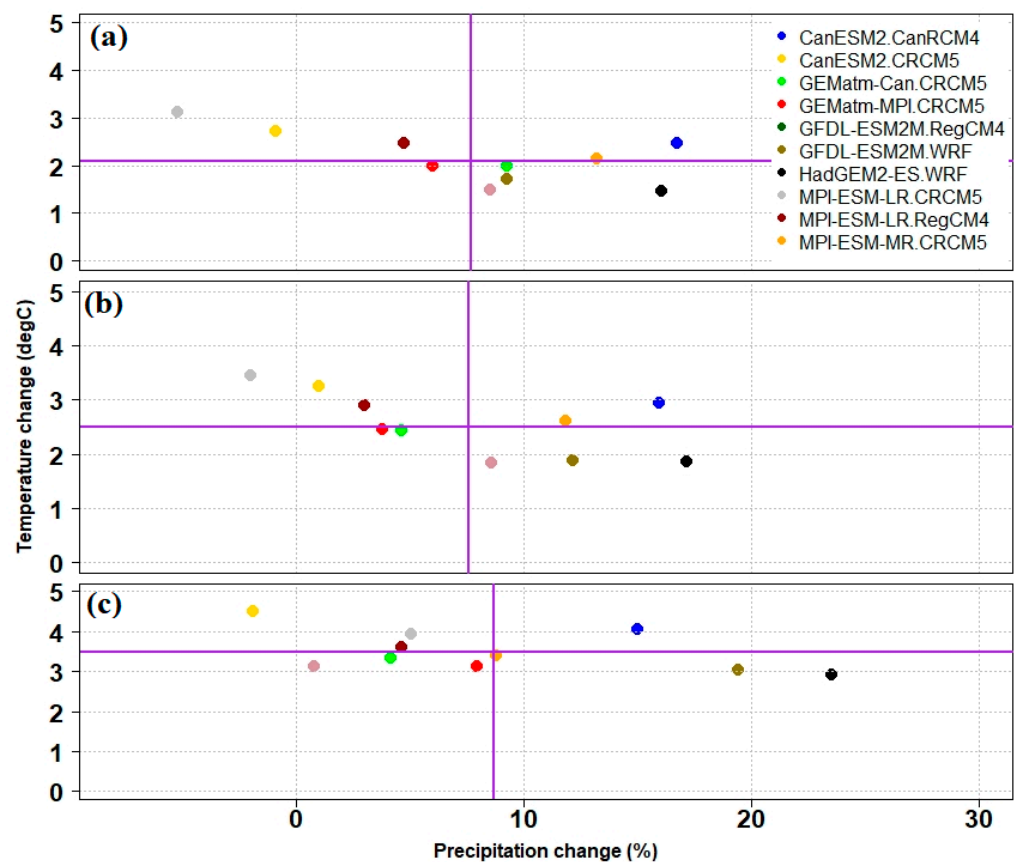


**Figure 6.** Scatter plots of annual changes in mean temperature and total precipitation in the region for 1.5 °C (a), 2 °C (b), and 3 °C (c). Purple lines give average of temperature and precipitation for all RCMs.

### 3.3. Impact of Climate Change on Drought

#### a. Meteorological drought

Figures 7–9 illustrate the time series of the 3-month long SPI, SPEI, and scPDSI for the historical baseline (1975–2004) and projections for the 30-year periods corresponding to each of the global warming scenarios. Most of the RCMs produce SPI values that suggest a future decrease in drought whereas the SPEI and PDSI give an increase in drought intensity.

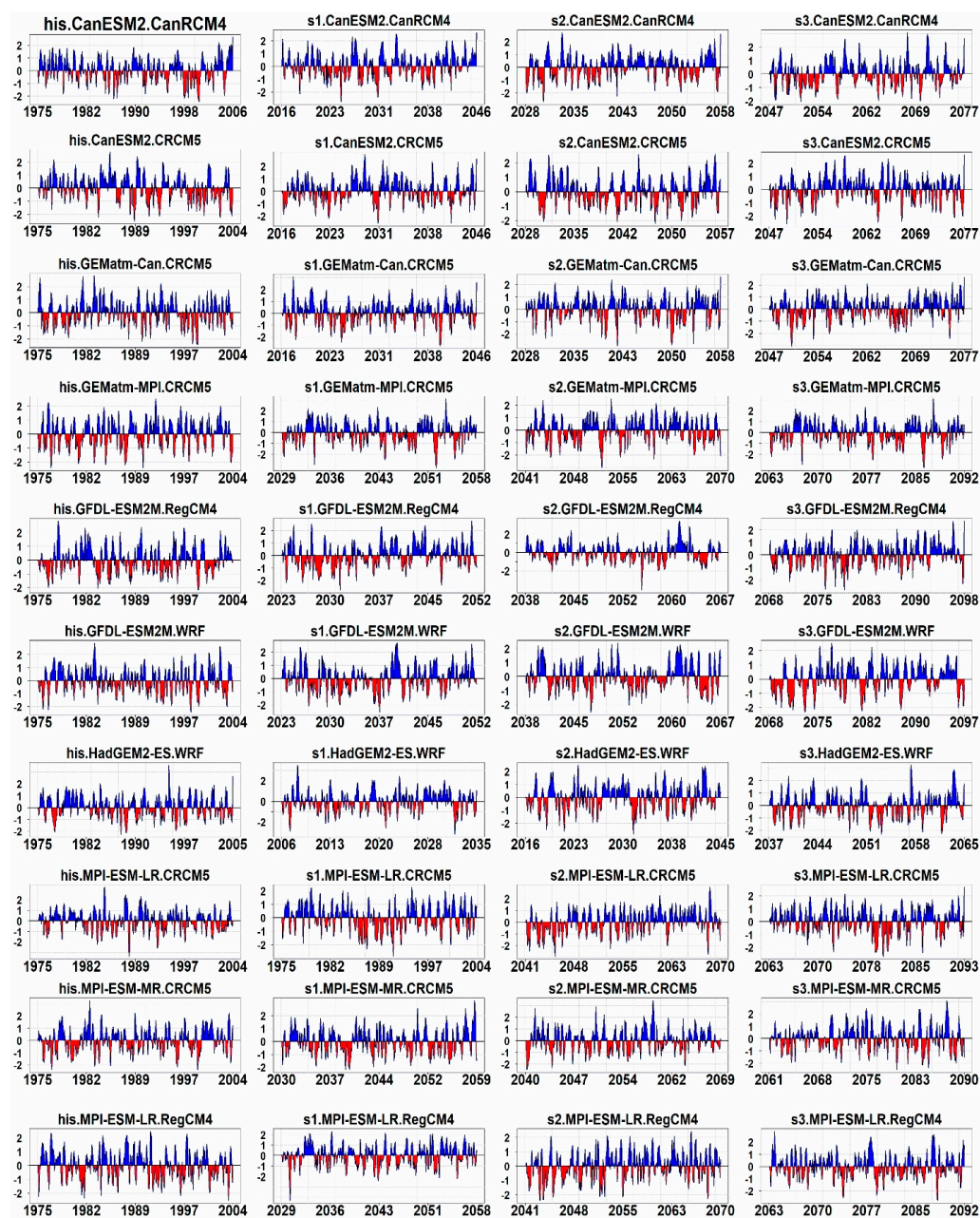


**Figure 7.** Time series of the SPI-3 for the historical baseline (1975–2004) and projections for each of the global warming scenarios.

The historical and future simulations of the PET results in this region indicated that during the historical period, the mean PET ranges from 194 to 224 mm, while it increases by 217–253, 220–260, and 222–270 mm for 1.5 °C, 2 °C, and 3 °C, respectively (Figure 10). The highest PET values (540 mm) in the projected period were produced by *ESM2.CRCM5* for the last scenario. The multi-RCM average PET was projected to increase by 10.5% at 1.5 °C, 12.6% at 2 °C, and 15.5% at 3 °C, relative to the historical period.

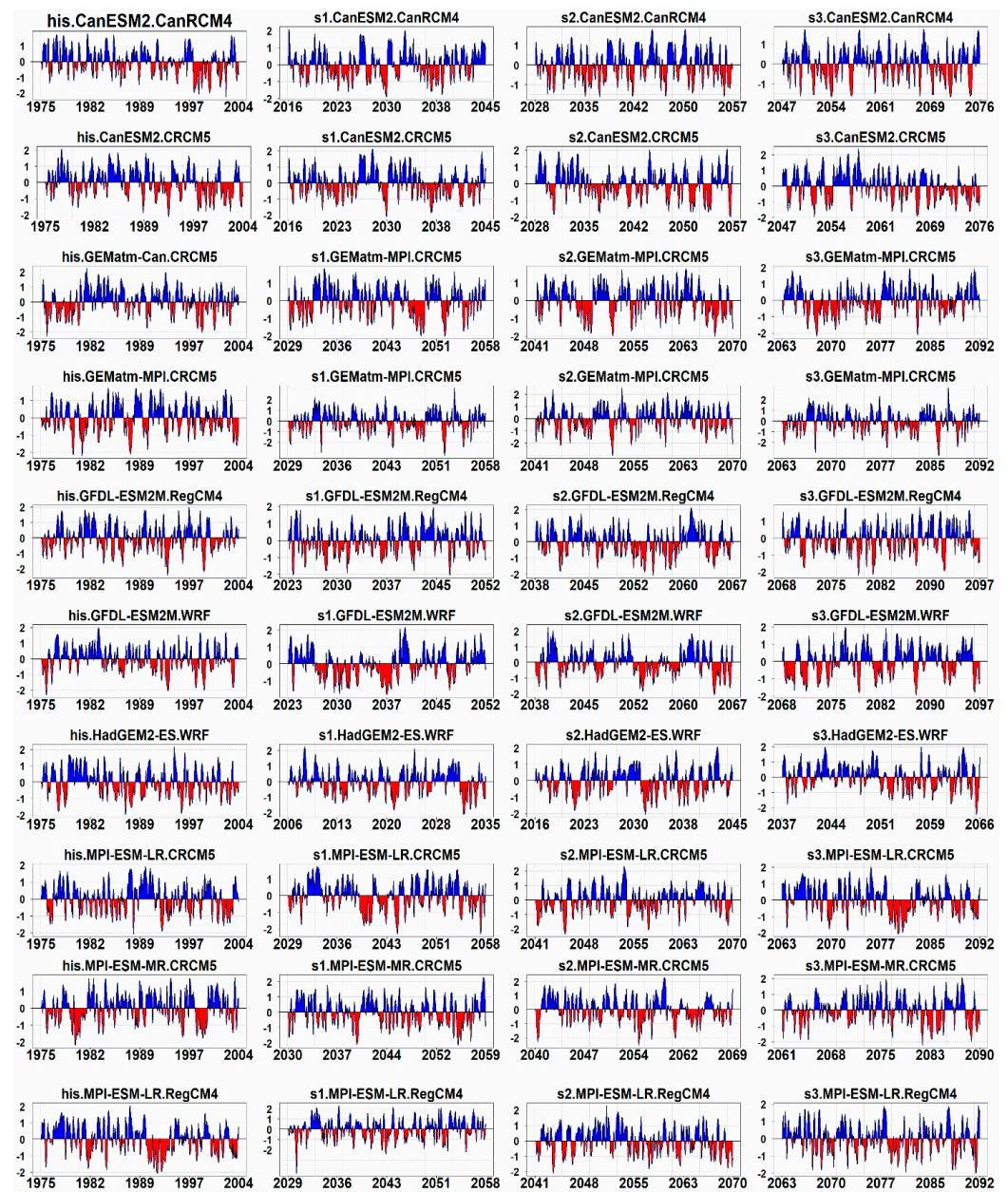


**Figure 8.** Time series of the SPEI-3 for the historical baseline (1975–2004) and projections for each of the global warming scenarios.

Figure 11 gives the number of drought events where the threshold level is at least moderate according to the SPI, SPEI, and scPDSI among all RCMs for the historical period and three global temperature scenarios (each period consists of 360 months). In the case of the SPEI, the mean number of droughts increases from 56 for the 1.5 °C scenario to 59 (2 °C), and then 68 (3 °C) when compared to the historical period (number of drought = 47). In the case of scPDSI, while the average number of droughts was 54, it increased to 65, 69, and 83 for 1.5 °C, 2 °C, and 3 °C, respectively. These results imply a noticeable increasing trend for the total number of drought events in the SSRB, although, the SPI data indicate 53, 56, and 53 months of drought for the 1.5 °C, 2 °C, and 3 °C scenarios, respectively, compared to 56 months for the historical period.

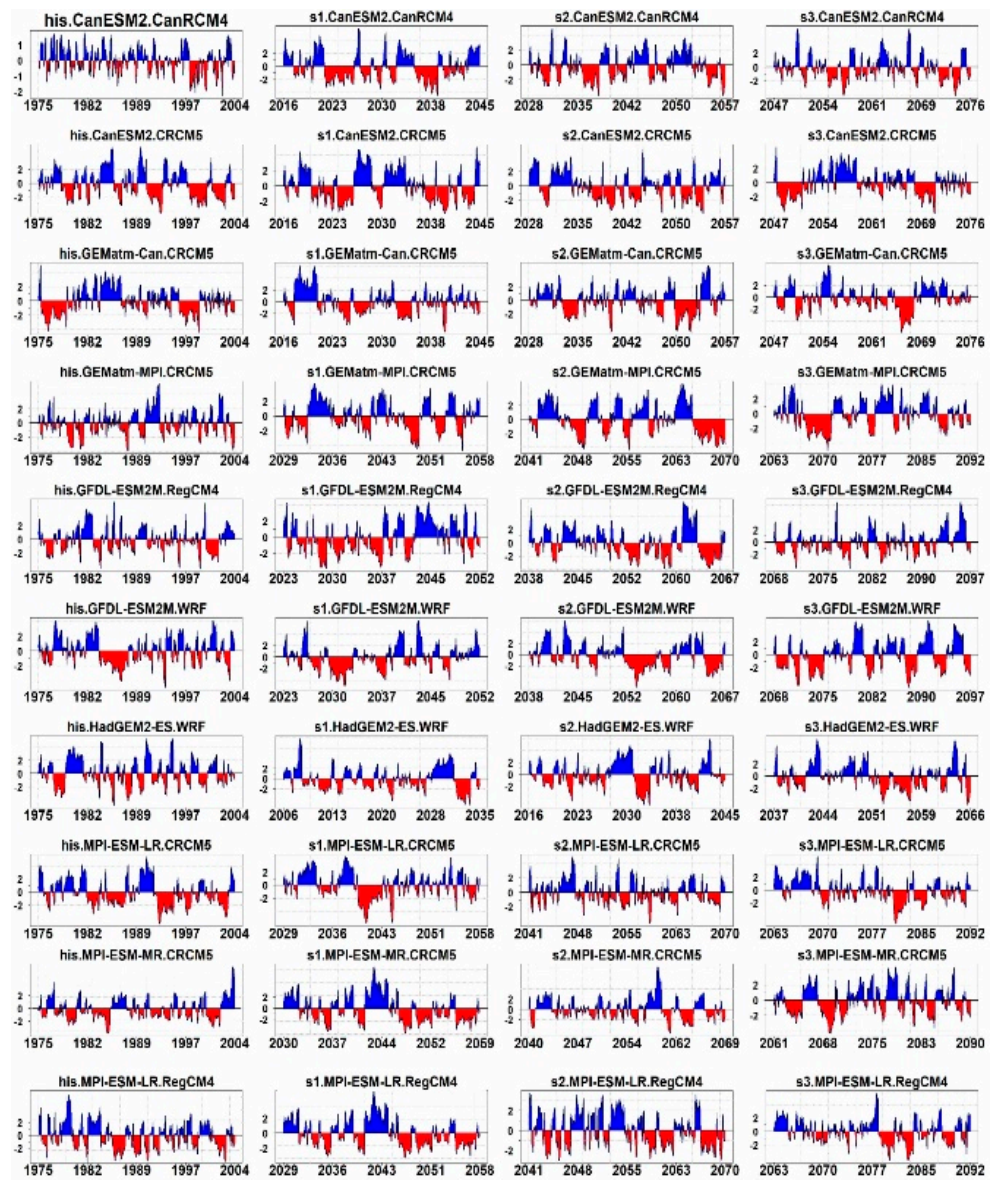


Figure 9. Time series of the scPDSI for the historical baseline (1975–2004) and projections for each of the global warming scenarios.

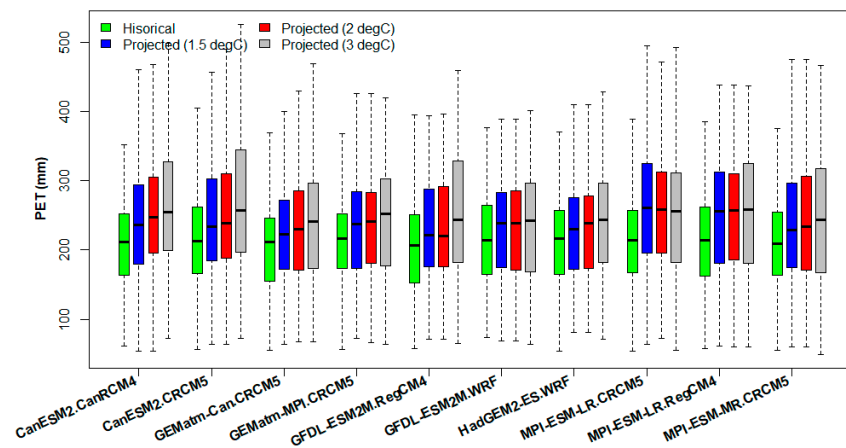
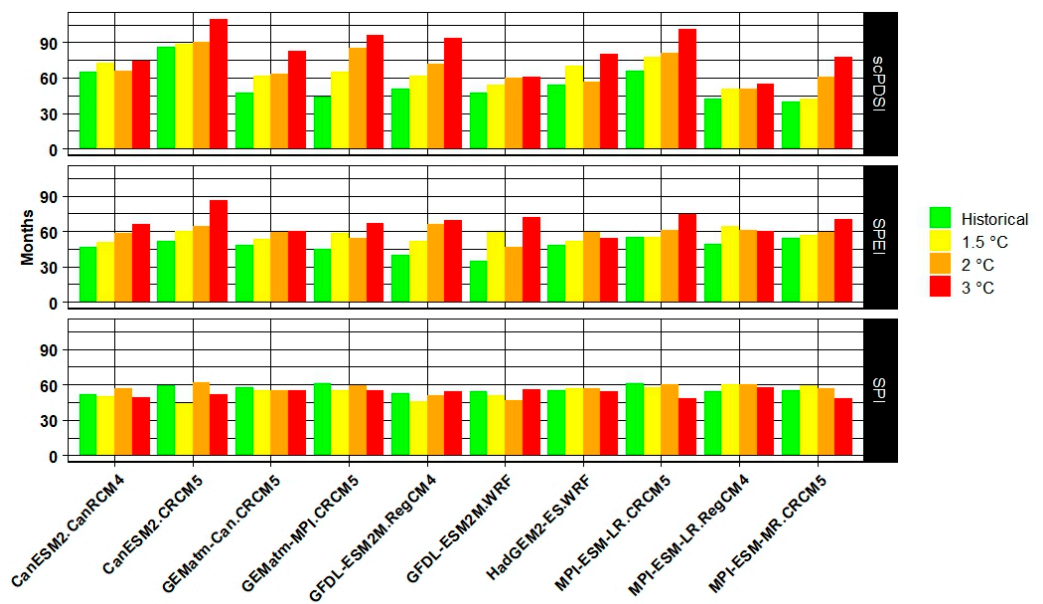
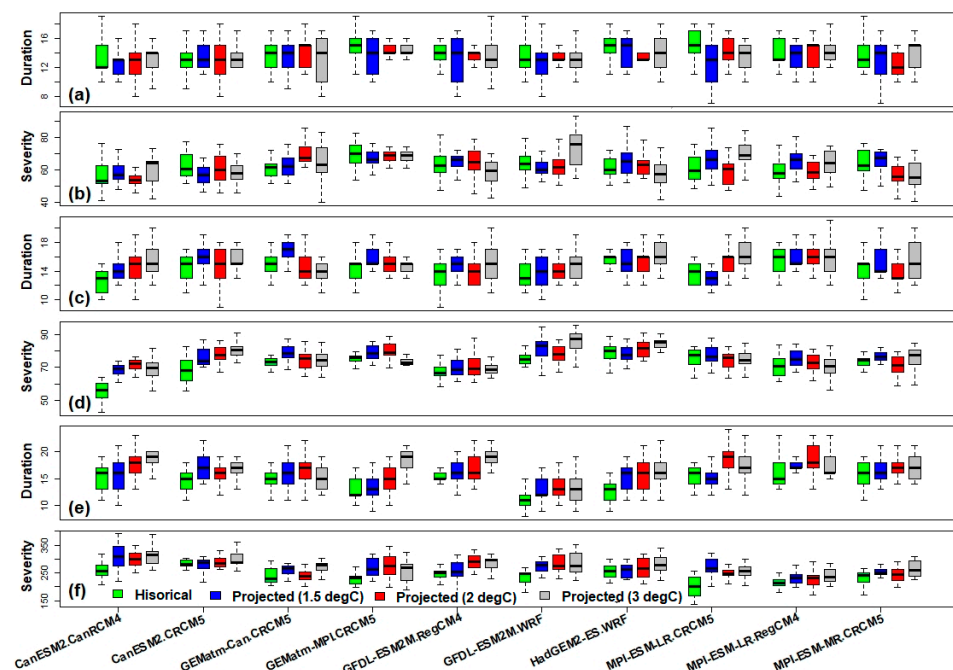


Figure 10. Temporally averaged of PET for the historical baseline (1975–2004) and projections for each of the global warming scenarios.



**Figure 11.** Total number of monthly drought events where the threshold level of SPEI, scPDSI, and SPI is at least moderate drought (−0.1 or below).

The results of drought duration and severity for 10 RCMs during the historical and projected periods at 17 weather stations show that the average historical drought duration for SPI was 14 months while this value was 13.2, 13.5, and 13.4 months in the first to third scenarios, respectively (Figure 12). The mean drought severity was 62.3 whereas it was 63.4, 61.6, and 63.5 in the first to third scenarios, respectively. Thus the SPI suggests that climate change has relatively little impact on drought severity and duration. The other drought indices give different results. For the SPEI, the average historical drought duration was 14.2, and in the first to third scenarios, it was 14.5, 15.2 and 16.4, respectively. The historical drought severity mean was an SPEI of 71; this increased to 74.5, 74, and 75.5 in the first to third scenarios, respectively. The scPDSI average drought duration was 14.4 months as opposed to 15.7, 16.4, and 17 in the first to third future scenarios, respectively.



**Figure 12.** Drought duration and severity for SPI (a,b), SPEI (c,d), and scPDSI (e,f).

b. Agricultural drought

We estimated the SMDI using simulated SWC from the SWAT model. Figure 13 illustrates the temporal evolution of the mean warm season SWC over the historical and projected periods under the three thresholds of global temperature change (30-year periods). The ensemble median SWC was 12.5% in the historical period while it decreased to 10.3%, 9.8%, and 8.2% in the first to third scenarios, respectively.

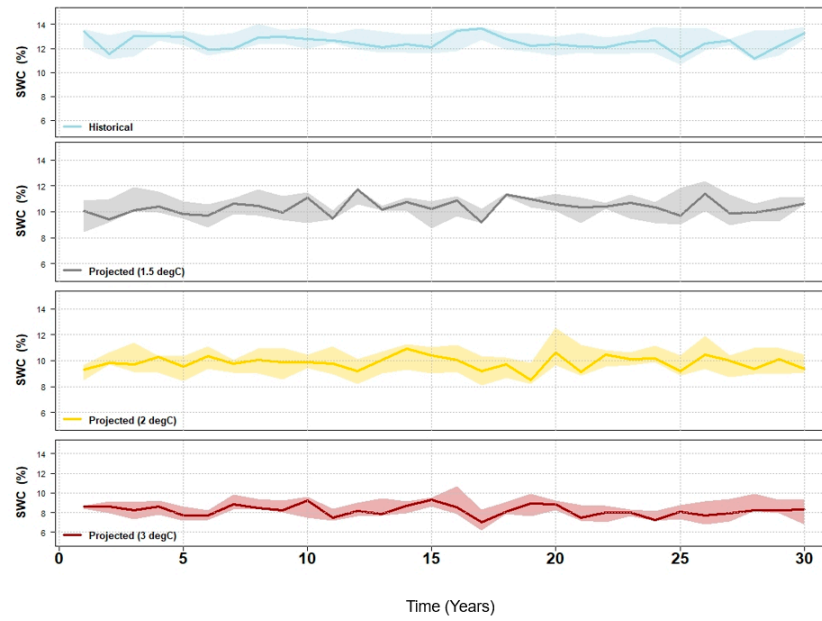


**Figure 13.** Soil water content during historical and three thresholds of temperature increases among all RCM model over the region. Solid lines show the ensemble medians and the shadings show the interquartile ensemble spread (25th and 75th quantiles).

The distributions of simulated changes in the SMDI during the historical and three future 30-year periods are presented as a boxplot in Figure 14. The mean historical SMDI was 1.04 and  $-0.26$ ,  $-0.56$ , and  $-1$  for the first to third future scenarios, respectively. Most of the SMDI data indicate near-severe drought under the 3 degree scenario with Canesm2.crcm5 showing the driest conditions among all RCMs. The 10 RCMs give a range of 3 to  $-0.54$  for the historical period and 2.6 to  $-2.8$ , 2.1 to  $-2.9$ , and 1.9 to  $-3$  for 1.5 °C, 2 °C and 3 °C, respectively.

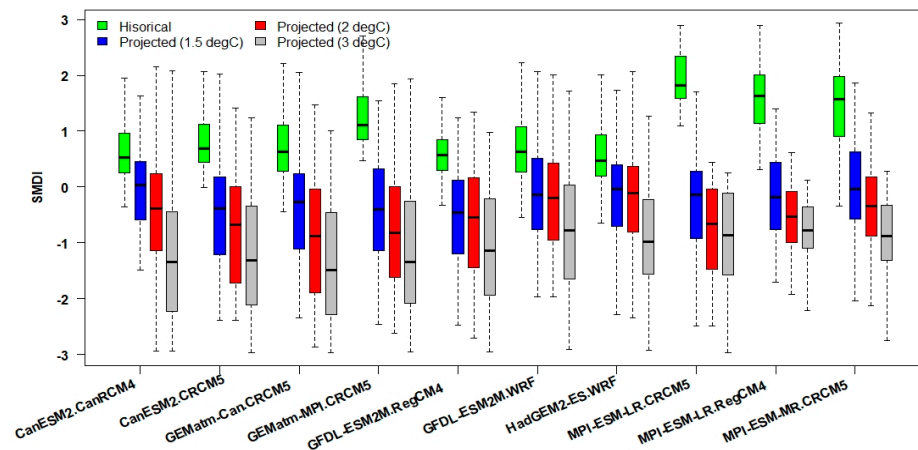


**Figure 14.** Box plots of the range of SMDI under historical and projected changes.

The spatial maps of the historical and projected average annual SMDI for the entire SSRB and for 10 RCMs revealed that the SMDI mean value ranges from  $-3.0$  to  $3.0$  over the basin (Figure 15). The lower elevations are more prone to drought risks than the higher elevations, with the exception of the western SSRB margin, which is an alpine ecosystem with thin soils. SMDI values decreased from historical to the last scenario, particularly for the two RCMs, MPI-ESM-LR.CRCM5 and CanESM2.CRCM5, while the historical SMDI map for GFDL-ESM2M.WRF shows the highest value. Overall, there is some similarity in the spatial patterns among SMDI maps with the intensification of agricultural drought, particularly for the  $3.0\text{ }^{\circ}\text{C}$  period, during which severe to extreme drought covered most of the basin.

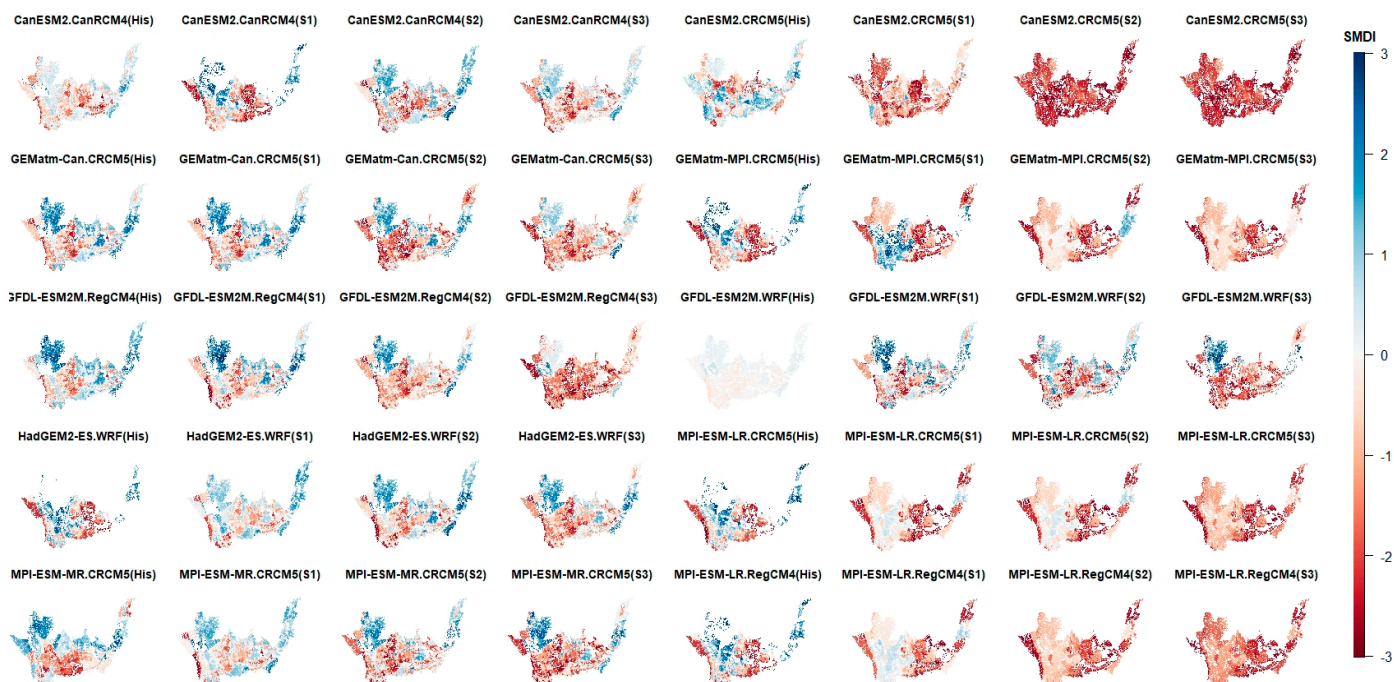


**Figure 15.** Spatial maps of average annual SMDI of the whole SSRB in historical and projections for 10 RCM model.

Figure 16 is a series of heat maps displaying temporal variations in the SMDI during the warm season (6 months) over the 30-year historical and projection periods (180 months) based on seven SMDI categories and the three thresholds of global temperature changes. These maps show that the number of dry months ( $\text{SMDI} = -1$  to  $-3$ ) is projected to be consistently higher than historical values. For instance, the number of months (average of all RCM model) in the near normal category ( $\text{SMDI} \sim 0$ ) was 106 historically, but it decreased to 99, 86, and 74 months for  $1.5\text{ }^{\circ}\text{C}$ ,  $2\text{ }^{\circ}\text{C}$ , and  $3\text{ }^{\circ}\text{C}$  of global warming, respectively. The RCMs simulate little or no severe and extreme drought during the historical period, with the exception of MPI-ESM-LR.CRCM5 and ESM-RL.Reg.CM4, which produce in less than 10 months of severe drought. Into the future, severe and extreme drought increase in frequency, while extremely wet and very wet conditions mostly disappear, especially with a  $3\text{ }^{\circ}\text{C}$  global temperature change.

The number of all dry months ( $-0.1$  or below) in SMDI increase from 40 for the  $1.5\text{ }^{\circ}\text{C}$  to 59 ( $2\text{ }^{\circ}\text{C}$ ) and then 89 ( $3\text{ }^{\circ}\text{C}$ ) (Figure 17). Moreover, The ETDI results show a change to drier conditions so that multi-model mean total number of droughts increases from 45 under the  $1.5\text{ }^{\circ}\text{C}$  scenario to 48 ( $2\text{ }^{\circ}\text{C}$ ), and then 63 ( $3\text{ }^{\circ}\text{C}$ ), when compared to the historical period (32).

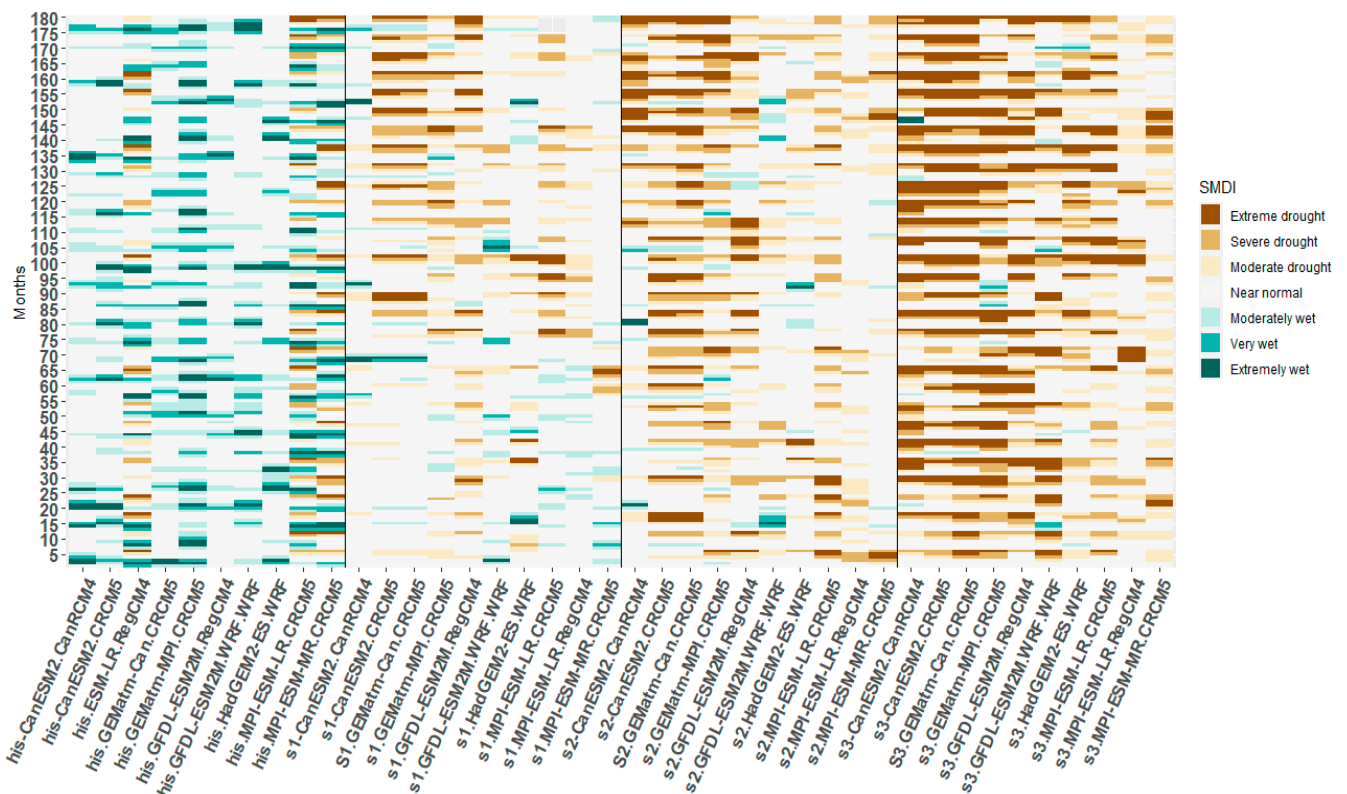


Figure 16. Temporal heat maps variations in the SMDI during the warm season over historical and projection.

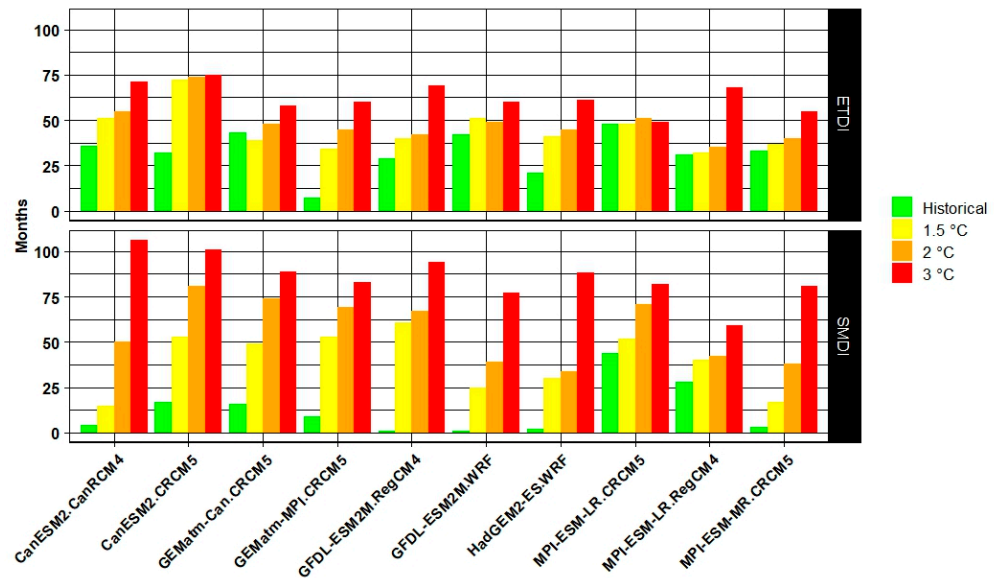


Figure 17. Total drought events of SMDI and ETDI where the threshold level is at least into the moderate drought ( $-0.1$  or below).

The distribution of simulated changes in ETDI for the 30-year historical baseline and projections are presented as a boxplot in Figure 18. The projected mean historical ETDI was 0.58 while this value fell to 0.2, 0.1, and  $-0.2$  in the first to third scenarios, respectively. ETDI values show mostly near-severe drought at the 3 °C level with Canesm2.crcm5 giving the driest conditions.

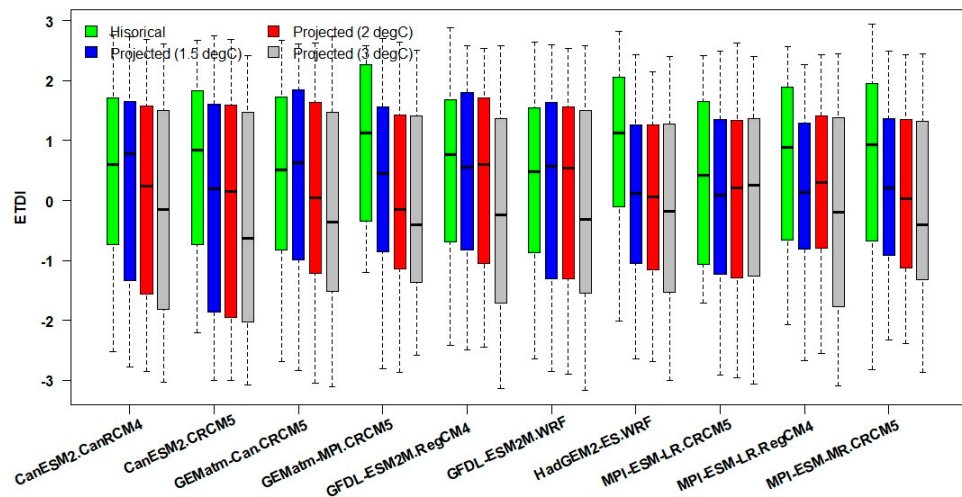


Figure 18. Box plots of the range of ETDI under historical and projected changes.

The warm season heat maps for seven categories of ETDI over the historical and projected periods (180 months) are given in Figure 19. Historically, the number of months (average of all RCMs) in the near normal category was 65, and it decreased to 59, 55, and 47 months for 1.5 °C, 2 °C, and 3 °C scenarios, respectively.

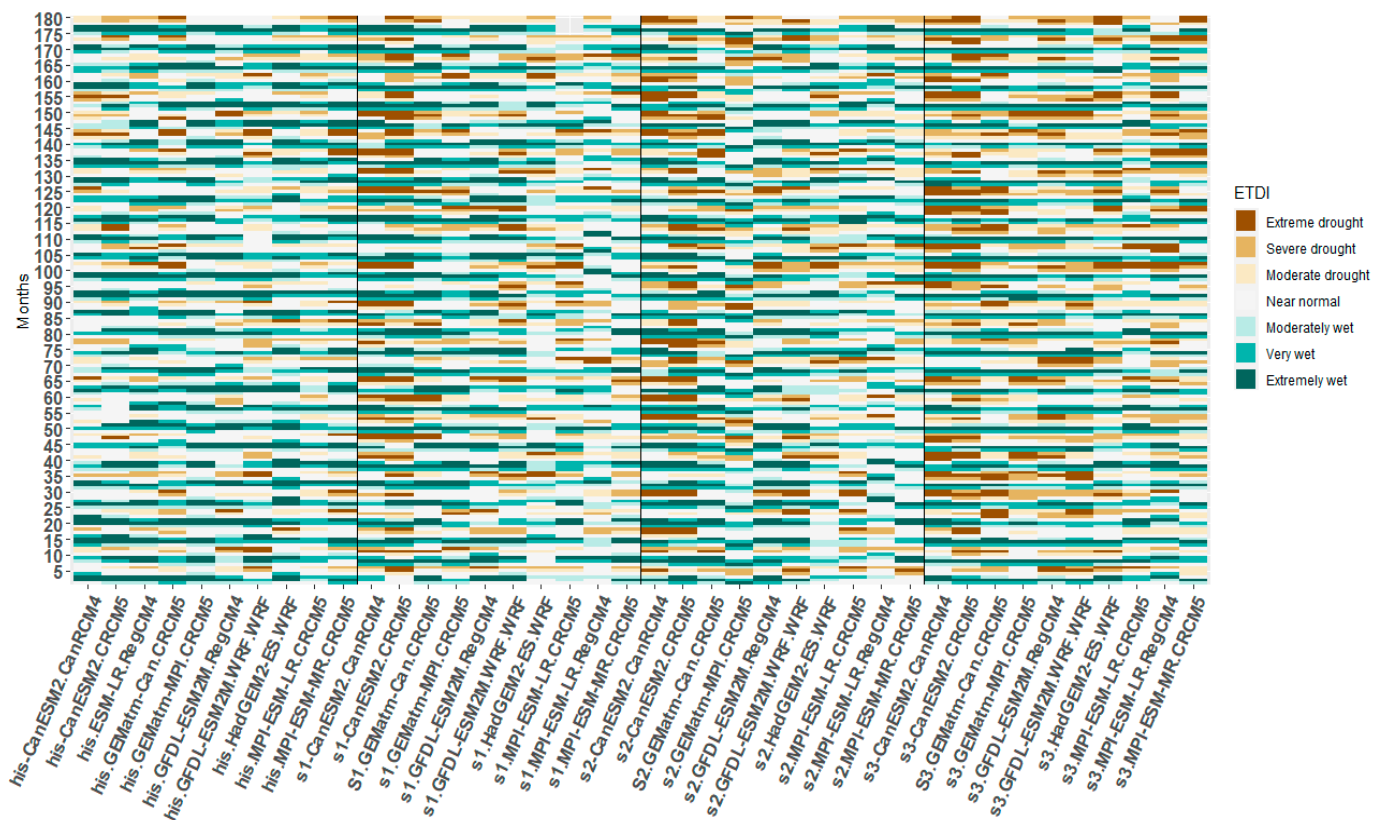
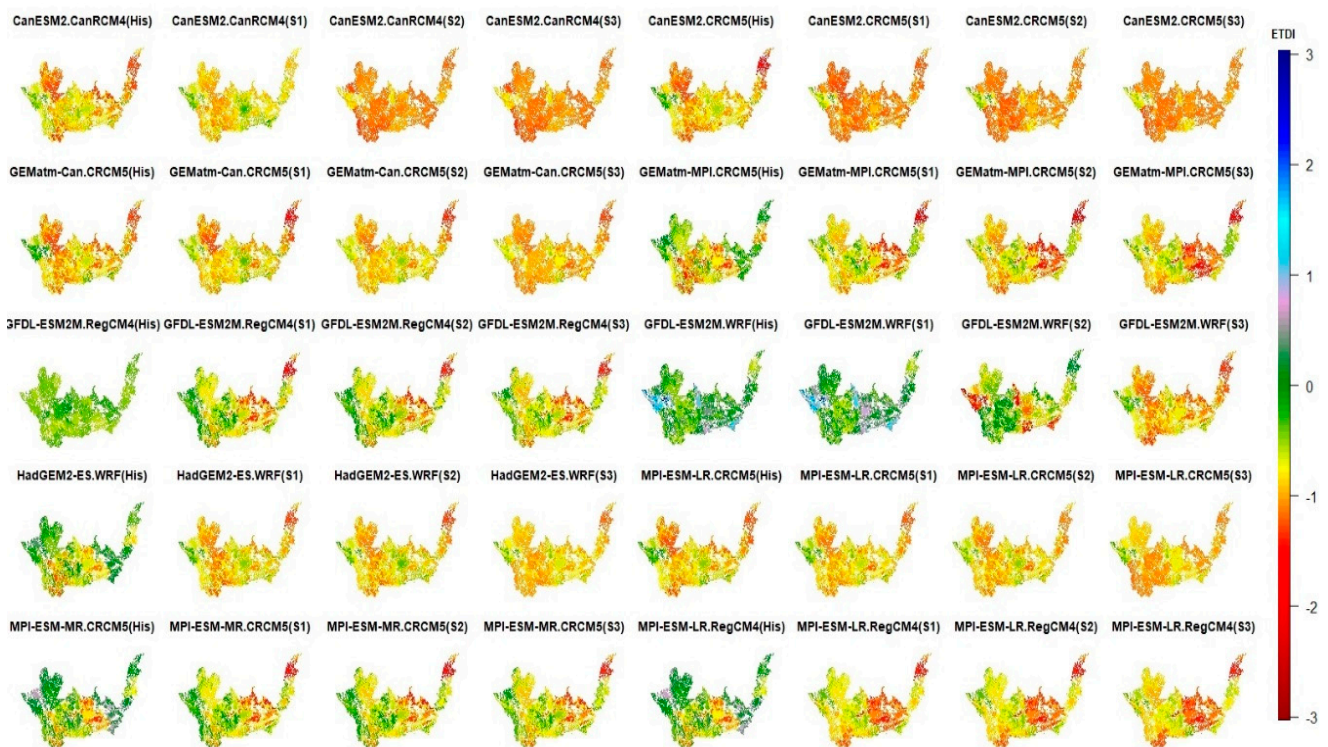


Figure 19. Temporal heat maps variations in the ETDI during the warm season over historical and projection.

The pattern of average ETDI for historical and projected periods indicates that the southern parts of the basin, particularly surrounding Lethbridge, Taber, Bow Island, and Medicine, tend to experience relatively more severe and extreme droughts (Figure 20).



**Figure 20.** Spatial maps of average annual ETDI of the whole SSRB in historical and projections for 10 RCM model.

#### 4. Discussion

The SWAT-M subroutine adequately predicted the streamflow and SWC relative to observational data in the cold region SSRB of western Canada. The main limitation of the SWAT model is that it simulates the streamflow and other hydrological components during the spring in the cold regions due to an abrupt increase during snowmelt in spring [26,65,66]. Therefore, SWAT source code needs to be modified in regions with cold climate and sparse rainfall as the snowmelt runoff is affected by temperature and climate change. SWAT-M module simulates freeze–thaw cycles and captures the effect of snow cover on ice-water content of the surface soil. This is based by combining an energy balance snowmelt equation with physically based soil temperature. Hence, we applied a combination of a physically based soil module (not empirical), with an energy budget equation for snowmelt during ROS events because it contributed to enhancing the accuracy for simulating daily SWC and monthly streamflow in this study.

Analysis of the future projected climate indicates that changes in annual mean temperature not only are positive for all RCMs but also are greater than the global mean temperature increase. This result is consistent with Tanzeeba and Gan [29], who reported a 2 °C increase for the mid-century and 2 °C to 4.5 °C for the late-century, and He et al. [67] who reported increases of 3.9, 3.6, and 3.5 °C for Swift Current, Saskatoon, and Melfort, respectively, for the mid-century. However, their findings were based on the GCM output. Our results from the RCMs of the NA-CORDEX climate model ensemble are characterized by an increase in annual precipitation, an increase in temperature, and consequently, an increase in evapotranspiration under three thresholds of temperature increases. Among the models, CanESM2.CRCM5 shows the driest conditions for both periods whereas HadGEM2-ES.WRF and GEMatm-MPI.CRCM5 have the wettest conditions for the near future and distant future, respectively.

The multi-RCM average PET was projected to increase by 10.5% at 1.5 °C, 12.6% at 2 °C, and 15.5% at 3 °C relative the historical period. Various studies suggest that the Prairies will warm faster than the global mean resulting in significant changes in the temperature and PET in the region [20–23, 26]. Intensification of future drought is revealed

by rising index values under almost all climate change scenarios. The exception is the precipitation-based SPI, since most projections show an increase in precipitation, SPI values do not change significantly in the future [68], while the scPDSI and SPEI, which incorporate temperature and PET, indicate a longer drought duration compared with SPI. Touma et al. [68], Nguvava et al. [69], and Haile et al. [70] reported similar findings with larger shifts in projected drought characteristics using the SPEI index than the SPI. Similarly, our results demonstrate the effect of temperature and PET as important determinants of future drought risks. Drought duration and severity derived from scPDSI data are generally greater than those based on the SPEI and SPI; however, there is no significant disparity between scPDSI and SPEI in drought duration. These results are consistent with the finding of Bonsal et al. [25], who noted increased severe drought conditions (higher SPEI) across the Prairies. Our results confirm an increase in the number of drought events and in drought duration and severity in long-term drought events in the SSRB by the end of the century. The SMDI and ETDI data show that the projected number of dry months is consistently higher than the historical results. At longer time scales, the drought heat maps in Figures 16 and 19 can be interpreted as a consequence of the cumulative effects of higher evapotranspiration and less soil moisture, particularly with a 3.0 °C increase in mean global temperature.

The spatial patterns of historical and projected SMDI and ETDI for the SSRB and 10 RCMs show that lower warmer elevations are more prone to drought risks. The notable exception is the thin alpine soils at the highest elevation on the western margin of the SSRB. SMDI and ETDI patterns are similar in terms of the range and scatter of values. This result is consistent with Masud et al. [71] who reported severe droughts in the middle parts of the basin, near the Alberta–Saskatchewan border, whereas they less severe droughts in the areas surrounding the Saskatchewan–Manitoba border. While the spatial pattern of the SMDI and ETDI had no obvious change between historical and projected periods, the index values sharply decline between the time slices representing three global temperature thresholds, with greatest severity with a 3 °C rise in global temperature. This result is consistent with Separovic et al. [72], Yang et al. [73], and Zare et al. [28] who reported drier soil moisture in the future compared to historical in the southern Canadian Prairies during the warm season. By accounting for the temperature, actual and potential evaporation, land cover, and relative soil moisture, the agricultural drought indices shows more significant effects toward the end of the century compared with meteorological drought. The SMDI in particular can consider long-term water stress in the root zone as a key indicator of the onset of agricultural drought. Generally, the distribution of SMDI and ETDI simulated values, illustrated by the spatial maps and heat maps, indicates that Canesm2.CRCM5 gives the driest condition among all RCMs.

## 5. Conclusions

In this study, we examined the implications of global warming for regional meteorological and agricultural drought in the SSRB. A global temperature threshold-based approach applies the different timing and rates of warming, according to temperature targets from international agreements to the regional conditions. Precipitation and temperature increase at different rates simulated by each regional climate model. Consequently, drought indices differ among models and levels of global warming. The analysis of three meteorological drought indices indicates that the scPDSI and SPEI give moderate, severe, and extremely dry conditions that are more frequent than with the SPI. Since most climate change scenarios show an increase in precipitation in the future, the precipitation-based SPI does not indicate significant changes in the drought intensity while the scPDSI and SPEI algorithms include temperature and PET. Estimates of the variables SWC, AET, and PET from the physically based SWAT model enabled the assessment of the agricultural drought indices SMDI and ETDI. The SWAT model employed a new algorithm for cold region hydrology and performed well; the range of SWC output was a good fit with observed SWC.

The results from our analysis of two agricultural drought indices, SMDI and ETDI, have major implications for Canada's agricultural economy and food security, given that the Prairie Provinces produce most of Canada's cereal, pulse and oil seed crops. Global warming could favor food production at high colder latitudes; however, taking advantage of a warmer climate will require adaptations of farming practice and technology to withstand a drier growing season. The degree and types of adaptation required will depend on the severity, geographic extent and duration of drought. Our study has determined how these characteristics of drought will change across a major agricultural river basin with 1.5, 2 and 3 °C of global warming.

In Canada's western interior, the adaptation of farming practices to a cold dry climate has produced one of world's most commercially viable agricultural economies. Much of this adaptation occurred in response to crop losses from periodic drought. The major and early adaptations included a network of reservoirs, canals, and pipelines to irrigate otherwise dry soils. Most of the irrigated land in Canada is in the SSRB. The results of our research indicate that the agricultural industry may rely heavily on irrigation to offset the projected increase in the intensity of drought. Offsetting the impacts of drought may also require changes to farming practices to maintain soil health for purpose of minimizing the loss of soil moisture. The worst-case future scenario for Canada's western interior is a long period of low precipitation in a warmer climate [27]. A sustained shortage of water for the irrigation of farmland, and other industrial and municipal uses of water, would require adaptations that extend beyond farming practices to policies that governs the use, allocation, and appointment of water.

**Author Contributions:** Data curation and analysis, M.Z.; supervision, S.A. and D.S.; writing—original draft, M.Z.; writing—review and editing, S.A., D.S. and S.B. All authors have read and agreed to the published version of the manuscript.

**Funding:** This research was funded by the Natural Science and Engineering Research Council of Canada (fund number is RGPIN-06456-2018).

**Institutional Review Board Statement:** Not applicable.

**Informed Consent Statement:** Not applicable.

**Data Availability Statement:** The authors can provide access to the modeling data upon request.

**Acknowledgments:** The authors thank the University of Regina and the Prairie Adaptation Research Collaborative for providing computational facilities.

**Conflicts of Interest:** The authors declare there are no conflict of interest.

## References

1. Marcos-Garcia, P.; Lopez-Nicolas, A.; Pulido-Velazquez, M. Combined use of relative drought indices to analyze climate change impact on meteorological and hydrological droughts in a Mediterranean basin. *J. Hydrol.* **2017**, *554*, 292–305. [\[CrossRef\]](#)
2. Heim, R.R. A review of twentieth-century drought indices used in the United States. *Bull. Am. Meteorol. Soc.* **2002**, *83*, 1149. [\[CrossRef\]](#)
3. Pielke, R.A.; Doesken, N.; Bliss, O.; Green, T.; Chaffin, C.; Salas, J.D.; Woodhouse, C.A.; Lukas, J.J.; Wolter, K. Drought 2002 in Colorado: An Unprecedented Drought or a Routine Drought? *Pure Appl. Geophys.* **2005**, *162*, 1455–1479. [\[CrossRef\]](#)
4. Naumann, G.; Alfieri, L.; Wyser, K.; Mentaschi, L.; Betts, R.A.; Carrao, H.; Spinoni, J.; Vogt, J.; Feyen, L. Global Changes in Drought Conditions Under Different Levels of Warming. *Geophys. Res. Lett.* **2018**, *45*, 3285–3296. [\[CrossRef\]](#)
5. Kim, T.-W.; Jehanzaib, M. Drought Risk Analysis, Forecasting and Assessment under Climate Change. *Water* **2020**, *12*, 1862. [\[CrossRef\]](#)
6. Aadhar, S.; Mishra, V. High-resolution near real-time drought monitoring in south Asia. *Sci. Data* **2017**, *4*, 170145. [\[CrossRef\]](#)
7. Aghakouchak, A.; Farahmand, A.; Melton, F.S.; Teixeira, J.; Anderson, M.C.; Wardlow, B.D.; Hain, C.R. Remote sensing of drought: Progress, challenges and opportunities. *Rev. Geophys.* **2015**, *53*, 452–480. [\[CrossRef\]](#)
8. Dai, A. Characteristics and trends in various forms of the Palmer Drought Severity Index during 1900–2008. *J. Geophys. Res.* **2011**, *116*, D12115. [\[CrossRef\]](#)
9. Bush, E.; Lemmen, D.S. *Canada's Changing Climate Report*; Government of Canada: Ottawa, ON, Canada, 2019; p. 444.
10. Kim, K.; Daly, E.J.; Flesch, T.K.; Coates, T.W. Carbon and water dynamics of a perennial versus an annual grain crop in temperate agroecosystems. *Agric. For. Meteorol.* **2022**, *314*, 108805. [\[CrossRef\]](#)

11. Sauchyn, D.; Barrow, E.; Fang, X.; Henderson, N.; Johnston, M.; Pomeroy, J.; Thorpe, J.; Wheaton, E.; Williams, B. *Saskatchewan Natural Capital in a Changing Climate: An Assessment of Impact and Adaptation*; Report to Saskatchewan Ministry of Environment; Prairie Adaptation Research Collaborative: Regina, SK, Canada, 2009; 162p.
12. Akhter, A.; Azam, S. Flood-drought hazard assessment for a flat clayey deposit in the Canadian Prairies. *J. Environ. Inform. Lett.* **2019**, *1*, 8–19. [[CrossRef](#)]
13. Loukas, A.; Vasiliades, L.; Tzabiras, J. Climate change effects on drought severity. *Adv. Geosci.* **2008**, *17*, 23–29. [[CrossRef](#)]
14. Wheeler, H.; Gobeil, P. Water security in the Canadian Prairies: Science and management challenges. *Philos. Trans. R. Soc. A* **2013**, *371*, 20120409. [[CrossRef](#)] [[PubMed](#)]
15. Farm Credit Canada (FCC), Technology Disruptors Study, FCC Vision October 2022. Available online: <https://www.fccvision.ca/> (accessed on 19 December 2022).
16. Chipanshi, A.C.; Findlater, K.M.; Hadwen, T.; O'Brien, E.G. Analysis of consecutive droughts on the Canadian prairies. *Clim. Res.* **2006**, *30*, 175–187. [[CrossRef](#)]
17. Bonsal, B.R.; Wheaton, E.E.; Chipanshi, A.C.; Lin, C.; Sauchyn, D.J.; Wen, L. Drought research in Canada: A review. *Atmos. Ocean* **2011**, *49*, 303–319. [[CrossRef](#)]
18. Sauchyn, D.; Ilich, N. Nine Hundred Years of Weekly Streamflows: Stochastic Downscaling of Ensemble Tree-Ring Reconstructions. *Water Resour. Res.* **2017**, *53*, 9266–9283. [[CrossRef](#)]
19. Akinremi, O.; McGinn, S.; Barr, A. Evaluation of the palmer drought index on the Canadian prairies. *J. Clim.* **1996**, *9*, 897–905. [[CrossRef](#)]
20. Quiring, S.M.; Papakryiakou, T.N. An evaluation of agricultural drought indices for the Canadian prairies. *Agric. For. Meteorol.* **2003**, *118*, 49–62. [[CrossRef](#)]
21. Roberts, E.; Stewart, R.E.; Lin, C.A. A study of drought characteristics over the Canadian Prairies. *Atmos. Ocean* **2006**, *44*, 331–345. [[CrossRef](#)]
22. Mkhabela, M.S.; Bullock, P.; Raj, S.; Wang, S.; Yang, Y. Crop yield forecasting on the Canadian Prairies using MODIS NDVI data. *Agr. Forest Meteorol.* **2011**, *151*, 385–393. [[CrossRef](#)]
23. Masud, M.B.; Qian, B.; Faramarzi, M. Performance of multivariate and multiscalar drought indices in identifying impacts on crop production. *Int. J. Climatol.* **2019**, *40*, 292–307. [[CrossRef](#)]
24. Masud, M.; Khaliq, M.; Wheeler, H. Future changes to drought characteristics over the Canadian Prairie Provinces based on NARCCAP multi-RCM ensemble. *Clim. Dyn.* **2017**, *48*, 2685–2705. [[CrossRef](#)]
25. Bonsal, B.; Liu, Z.; Wheaton, E.; Stewart, R. Historical and projected changes to the stages and other characteristics of severe Canadian Prairie droughts. *Water* **2020**, *12*, 3370. [[CrossRef](#)]
26. Zare, M.; Azam, S.; Sauchyn, D. Evaluation of Soil Water Content Using SWAT for Southern Saskatchewan, Canada. *Water* **2022**, *14*, 249. [[CrossRef](#)]
27. Tanzeeba, S.; Gan, T.Y. Potential impact of climate change on the water availability of South Saskatchewan River Basin. *Clim. Chang.* **2012**, *112*, 355–386. [[CrossRef](#)]
28. Zare, M.; Azam, S.; Sauchyn, D. A Modified SWAT Model to Simulate Soil Water Content and Soil Temperature in Cold Regions: A Case Study of the South Saskatchewan River Basin in Canada. *Sustainability* **2022**, *14*, 10804. [[CrossRef](#)]
29. Sauchyn, D.; Davidson, D.; Johnston, M. Prairie Provinces; Chapter 4. In *Canada in a Changing Climate: Regional Perspectives, Report*; Warren, F.J., Lulham, N., Lemmen, D.S., Eds.; Government of Canada: Ottawa, ON, Canada, 2020.
30. Lac, S. A Climate change adaptation study for the South Saskatchewan River Basin. In *SSHRC MCRI-Institutional Adaptation to Climate Change Project*; Canadian Plains Research Centre, University of Regina: Regina, SK, Canada, 2004.
31. Masud, M.B.; McAllister, T.; Cordeiro, M.R.C.; Faramarzi, M. Modeling future water footprint of barley production in Alberta, Canada: Implications for water use and yields to 2064. *Sci. Total Environ.* **2018**, *616*, 208–222. [[CrossRef](#)] [[PubMed](#)]
32. Giorgi, F.; Jones, C.; Asrar, G. Addressing climate information needs at the regional level: The CORDEX framework. *WMO Bull.* **2009**, *58*, 175–183.
33. Mearns, L.; McGinnis, S.; Korytina, D.; Arritt, R. The NA-CORDEX Dataset, Version 1.0. NCAR Climate Data Gateway, Boulder CO. 2017. Available online: <https://doi.org/10.5065/D6SJ1JCH> (accessed on 16 May 2017). [[CrossRef](#)]
34. McKee, T.B.; Doesken, N.J.; Kleist, J. The relationship of drought frequency and duration to time scales. In *Proceedings of the Eighth Conference on Applied Climatology*, Anaheim, CA, USA, 17–22 January 1993.
35. Ogunrinde, A.T.; Oguntunde, P.G.; Akinwumiju, A.S.; Fasinmirin, J.T. Evaluation of the Impact of Climate Change on the Characteristics of Drought in Sahel Region of Nigeria: 1971–2060. *Afr. Geogr. Rev.* **2021**, *40*, 192–210. [[CrossRef](#)]
36. Jehanzaib, M.; Yoo, J.; Kwon, H.-H.; Kim, T.-W. Reassessing the frequency and severity of meteorological drought considering non-stationarity and copula-based bivariate probability. *J. Hydrol.* **2021**, *603*, 126948. [[CrossRef](#)]
37. Vicente-Serrano, S.M.; Begueria, S.; Lopez-Moreno, J.I. A multiscalar drought index sensitive to global warming: The Standardized Precipitation Evapotranspiration Index. *J. Clim.* **2010**, *23*, 1696–1718. [[CrossRef](#)]
38. Nam, W.H.; Hayes, M.J.; Wilhite, D.A.; Svoboda, M.D. Projection of temporal trends on drought characteristics using the standardized precipitation evapotranspiration index (SPEI) in South Korea. *J. Kor. Soc. Agri. Eng.* **2015**, *57*, 37–45.
39. Jiang, R.; Xie, J.; He, H.; Luo, J.; Zhu, J. Use of four drought indices for evaluating drought characteristics under climate change in Shaanxi, China: 1951–2012. *Nat. Hazard.* **2015**, *75*, 2885–2903. [[CrossRef](#)]

40. Ahmadalipour, A.; Moradkhani, H.; Yan, H.; Zarekarizi, M. Remote Sensing of Drought: Vegetation, Soil Moisture and Data Assimilation, Remote Sensing of Hydrological Extremes. In *Remote Sensing of Hydrological Extremes*; Springer International Publishing: Cham, Switzerland, 2017; pp. 121–149.
41. Wang, H.; Chen, Y.; Pan, Y.; Chen, Z.; Ren, Z. Assessment of candidate distributions for SPI/SPEI and sensitivity of drought to climatic variables in China. *Int. J. Clim.* **2019**, *39*, 4392–4412. [[CrossRef](#)]
42. Guttman, N.B. Accepting the standardized precipitation index: A calculation algorithm. *J. Am. Water Resour. Assoc.* **1999**, *35*, 311–322. [[CrossRef](#)]
43. Abramowitz, M.; Stegun, I.A. *Handbook of Mathematical Functions*. Dover Publications: New York, NY, USA, 1965.
44. Wells, N.; Goddard, S.; Hayes, M.J. A self-calibrating Palmer drought severity index. *J. Clim.* **2004**, *17*, 2335–2351. [[CrossRef](#)]
45. Palmer, W.C. *Meteorological Drought, Research Paper No. 45*; U.S. Department of Commerce Weather Bureau: Washington, DC, USA, 1965.
46. Narasimhan, B.; Srinivasan, R. Development and evaluation of Soil Moisture Deficit Index (SMDI) and Evapotranspiration Deficit Index (ETDI) for agricultural drought monitoring. *Agric. For. Meteorol.* **2005**, *133*, 69–88. [[CrossRef](#)]
47. Mishra, A.K.; Singh, V.P. A review of drought concepts. *J. Hydrol.* **2010**, *391*, 202–216. [[CrossRef](#)]
48. Spinoni, J.; Naumann, G.; Carrao, H.; Barbosa, P.; Vogt, J. World drought frequency, duration, and severity for 1951–2010. *Int. J. Climatol.* **2014**, *34*, 2792–2804. [[CrossRef](#)]
49. Tan, C.; Yang, J.; Li, M. Temporal-spatial variation of drought indicated by SPI and SPEI in Ningxia Hui Autonomous region, China. *Atmosphere* **2015**, *6*, 1399–1421. [[CrossRef](#)]
50. Arnold, J.G.; Moriasi, D.N.; Gassman, P.W.; Abbaspour, K.C.; White, M.J.; Srinivasan, R.; Santhi, C.; Harmel, R.D.; Van Griensven, A.; Van Liew, M.W.; et al. SWAT: Model use, calibration, and validation. *Trans. ASABE* **2012**, *55*, 1491–1508. [[CrossRef](#)]
51. Mapfumo, E.; Chanasyk, D.S.; Willms, W.D. Simulating daily soil water under foothills fescue grazing with the Soil and Water Assessment Tool model (Alberta, Canada). *Hydrol. Process.* **2004**, *18*, 2787–2800. [[CrossRef](#)]
52. Refsgaard, J.C.; Storm, B. MIKE-SHE. In *Computer Models of Watershed Hydrology*; Singh, V.J., Ed.; Water Resources Pub.: Englewood, CO, USA, 1995; pp. 809–846.
53. Abbaspour, K.C.; Yang, J.; Maximov, I.; Siber, R.; Bogner, K.; Mieleitner, J.; Zobrist, J.; Srinivasan, R. Modelling hydrology and water quality in the pre-alpine/alpine Thur watershed using SWAT. *J. Hydrol.* **2007**, *333*, 413–430. [[CrossRef](#)]
54. Nash, J.E.; Sutcliffe, J.V. River flow forecasting through conceptual models: Part I—A discussion of principles. *J. Hydrol.* **1970**, *10*, 282–290. [[CrossRef](#)]
55. Moriasi, D.N.; Arnold, J.G.; Van Liew, M.W.; Binger, R.L.; Harmel, R.D.; Veith, T. Model evaluation guidelines for systematic quantification of accuracy in watershed simulations. *Trans. ASABE* **2007**, *50*, 885–900. [[CrossRef](#)]
56. Legates, D.R.; McCabe, G.J. Evaluating the use of “goodness-of-fit” measures in hydrologic and hydroclimatic model validation. *Water Resour. Res.* **1999**, *35*, 233–241. [[CrossRef](#)]
57. Rücker, A.; Boss, S.; Kirchner, J.W.; von Freyberg, J. Monitoring snowpack outflow volumes and their isotopic composition to better understand streamflow generation during rain-on-snow events. *Hydrol. Earth Syst. Sci. Discuss.* **2019**, *23*. [[CrossRef](#)]
58. Mamo, K.H.M.; Jain, M.K. Runoff and sediment modeling using SWAT in Gumera catchment, Ethiopia. *Open J. Mod. Hydrol.* **2013**, *3*, 38391.
59. Gyamfi, C.; Ndambuki, J.M.; Salim, R.W. A historical analysis of rainfall trend in the Olifants Basin in South Africa. *Earth Sci. Res.* **2016**, *5*, 129–142. [[CrossRef](#)]
60. Khalid, K.; Ali, M.F.; Rahman, N.F.A.; Mispan, M.R.; Haron, S.H.; Othman, Z.; Bachok, M.F. Sensitivity analysis in watershed model using SUFI-2 algorithm. *Procedia Eng.* **2016**, *162*, 441–447. [[CrossRef](#)]
61. Thavhana, M.P.; Savage, M.J.; Moeletsi, M.E. SWAT model uncertainty analysis, calibration and validation for runoff simulation in the Luvuvhu River catchment, South Africa. *Phys. Chem. Earth.* **2018**, *105*, 115–124. [[CrossRef](#)]
62. Moriasi, D.N.; Gitau, M.W.; Pai, N.; Daggupati, P. Hydrologic and water quality models: Performance measures and evaluation criteria. *Trans. ASABE* **2015**, *58*, 1763–1785.
63. Pomeroy, J.; Fang, X.; Williams, B. *Impacts of Climate Change on Saskatchewan’s Water Resources*; Centre for Hydrology, University of Saskatchewan: Saskatoon, SK, Canada, 2009.
64. Qi, J.; Zhang, X.; Wang, Q. Improving hydrological simulation in the Upper Mississippi River Basin through enhanced freeze-thaw cycle representation. *J. Hydrol.* **2019**, *571*, 605–618. [[CrossRef](#)]
65. Lévesque, É.; Anctil, F.; Van Griensven, A.N.N.; Beauchamp, N. Evaluation of streamflow simulation by SWAT model for two small watersheds under snowmelt and rainfall. *Hydrol. Sci. J.* **2008**, *53*, 961–976. [[CrossRef](#)]
66. Liang, K.; Jiang, Y.; Qi, J.; Fuller, K.; Nyiraneza, J.; Meng, F.R. Characterizing the impacts of land use on nitrate load and water yield in an agricultural watershed in Atlantic Canada. *Sci. Total Environ.* **2020**, *729*, 138793. [[CrossRef](#)] [[PubMed](#)]
67. He, Y.; Wang, H.; Qian, B.; McConkey, B.; DePauw, R. How early can the seeding dates of spring wheat be under current and future climate in Saskatchewan, Canada? *PLoS ONE* **2012**, *7*, e45153. [[CrossRef](#)]
68. Touma, D.; Ashfaq, M.; Nayak, M.A.; Kao, S.-C.; Diffenbaugh, N.S. A multi-model and multi-index evaluation of drought characteristics in the 21st century. *J. Hydrol.* **2015**, *526*, 196–207. [[CrossRef](#)]
69. Nguvava, M.; Abiodun, B.J.; Otieno, F. Projecting drought characteristics over East African basins at specific global warming levels. *Atmos. Res.* **2019**, *228*, 41–54. [[CrossRef](#)]

70. Haile, G.G.; Tang, Q.; Hosseini-Moghari, S.M.; Liu, X.; Gebremicael, T.G.; Leng, G.; Kebede, A.; Xu, X.; Yun, X. Projected impacts of climate change on drought patterns over East Africa. *Earths Future* **2020**, *8*, e2020EF001502. [[CrossRef](#)]
71. Masud, M.B.; Khaliq, M.N.; Wheeler, H.S. Analysis of meteorological droughts for the Saskatchewan River basin using univariate and bivariate approaches. *J. Hydrol.* **2015**, *522*, 452–466. [[CrossRef](#)]
72. Šeparović, L.; Alexandru, A.; Laprise, R.; Martynov, A.; Sushama, L.; Winger, K.; Tete, K.; Valin, M. Present Climate and Climate Change over North America as Simulated by the Fifth-Generation Canadian Regional Climate Model; Springer: Berlin/Heidelberg, Germany, 2013; Volume 41. ISBN 003820131 7375.
73. Yang Kam Wing, G.; Sushama, L.; Diro, G.T. The intraannual variability of land-atmosphere coupling over North America in the Canadian Regional Climate Model (CRCM5). *J. Geophys. Res. Atmos.* **2016**, *121*, 13859–13885. [[CrossRef](#)]

**Disclaimer/Publisher’s Note:** The statements, opinions and data contained in all publications are solely those of the individual author(s) and contributor(s) and not of MDPI and/or the editor(s). MDPI and/or the editor(s) disclaim responsibility for any injury to people or property resulting from any ideas, methods, instructions or products referred to in the content.